Tommy Dam
LTH
Master of Science in Engineering, Engineering Nanoscience

Constructing supported lipid bilayers from native cell membranes

Supervisor
Peter Jönsson
Division of Physical Chemistry, Lund University

Examiner
Emma Sparr
Division of Physical Chemistry, Lund University

LUNDS UNIVERSITET
Lunds Tekniska Högskola

Preface

This Master thesis concludes my education in the Engineering Nanoscience programme, with a specialisation in Nanobiomedicin, at LTH. The work was done at the Division of Physical Chemistry at Lund University during the spring of 2018. I found great interest in this work due to the combined disciplines of physics, biology and chemistry and I feel grateful for having been able to work on such an exciting project.

The experimental protocol presented in this work is adapted from the works of Dr Hudson Pace and Dr Marta Bally at Chalmers University. I would therefore like to express my thanks and gratitude to them and their research group for allowing me to visit the department of Applied Physics and helping me with understanding the protocol as well as providing me with all the essential vesicle samples. Thank you to Dr Mohammad Arif Kamal for accompanying me and helping me further understand the subject. A big thank you to my supervisor, Peter Jönsson, for introducing me to this topic, for explaining it so clearly and for the supervision and guidance throughout the project. I am still baffled by his dedication to supervision. Deepest gratitude to Vicky Junghans for all the helpful discussions which resulted in me understanding the subject a bit more, helping me with the experiments, introducing me to cell work and for always showing support. For helping me with all my confusion and turmoil when I'm working on the microscope, thank you Alexandra for your teachings and for your support. And thank you both for being such awesome office mates and for making these couple of months so much fun! Lastly, I would like to extend a special thanks to my family and friends for all the support.

Popular Science Summary

Mimicking the cell membrane

The cell membrane plays an important part in many of the cell's functions. It forms a boundary between the internal and external environment of the cell and governs the exchange of essential molecules, for the cell's survival, with its surroundings. The behaviour of the membrane and the proteins present in it, greatly affects our immune system and health. In fact, a majority of drugs in the market target some protein integrated into the cell membrane. With the presence of certain proteins embedded into the membrane, the cells in the immune system are able to communicate with each other to fight back any pathogens posing a threat against the body. The T-cell is one such cell in the immune system which is central in forming an immune response against bacteria or viruses.

Studying the cell membrane and the molecules therein can therefore seem to be an obvious endeavour but is quite difficult since it is so complex. For example, there are more than 600 lipid types in most cell membranes and the contribution from each cell membrane component can be hard to quantify. A popular alternative within research has been to instead use *supported lipid bilayers (SLBs),* a mimic of a real cell membrane formed on a solid support. Contrary to cell membranes, the SLB is comprised of only one or two lipid types and normally only have one type of membrane protein integrated into it. This makes it easier to study the function of individual proteins. Although this system has been of great use to study how membranes behave, it is in some instances too simple when compared to a live cell membrane. The main aim of this work has been to try and form SLBs which contain a larger fraction of lipids and membrane proteins that are naturally occurring in native cell membranes. Specifically, I tried to produce SLBs that resemble the cell membrane of the immune cells called T cells.

This was done by forming structures called *vesicles*. These structures can be imagined as planar bilayer, a membrane, which closes in on itself to form a sphere. One of the main tasks was to try and incorporate components from a real T cell membrane into these vesicle structures. This was done by optimizing a technique called *sonication*. When the vesicles are deposited onto a solid support, they deform and rupture to form a patch of SLB. In a real cell membrane, the lipids and proteins are able to move around in the bilayer. It is therefore interesting to investigate how fast the components are moving in the more cell-like SLB compared to the traditional SLBs which doesn't contain any components from real cell membranes. The results show that the lipids move a bit slower in the more cell-like SLB. Similar to how it is more difficult to move around in a more crowded room, the lipids move slower when facing more obstacles from the extra added components into bilayer from a real cell membrane.

I further investigated how much the SLB resembled the T-cell membrane by using *antibodies*. Antibodies are proteins which only bind specifically to a certain protein. By using antibodies I could detect if the membrane proteins one would expect to find on the membrane of a T cell, are present on the newly formed SLB. A few proteins could be detected on the surface of the SLB. However, the proteins seem to be quite stationary and does not move around very well. This problem is multi-facetted can be because the proteins are very large and

more massive objects require more energy to move around. An additional reason may be that the proteins are still part of vesicles which haven't ruptured, in which case they are not able to move in the bilayer that has formed.

In summation, this has been an investigation into whether it is possible to create a platform to better model the cell membrane of a T cell. An experimental protocol to produce a SLB, with cell membrane components, was formed. Although the membrane proteins seem to be largely stationary, the resulting SLB could still be used to study the binding mechanism of the proteins in the SLB which does not require proteins to move. This work forms a basis which could be further expanded upon to improve the produced cell-like SLB. The tool could then be used to further study how T cells interact with other cells in the immune system, giving more insights into how the body fights off diseases. Knowing more about this process could also optimize and improve some of the strategies, used by the pharmaceutical industry, developing drugs against a certain illness.

Abstract

The aim of this MSc-project was to investigate whether it is possible to incorporate native cell membrane components from Jurkat T cells into *supported lipid bilayers, SLBs,* to produce a model membrane system better resembling the native cell membranes in T cells. The procedure of forming *native-like SLBs (nSLB)* was adapted from an existing protocol and is done through the deposition of *hybrid vesicles* onto a cleaned glass slide. The hybrid vesicles are composed of synthetic lipids (PEGylated lipids and POPC) and native cell membrane components from the Jurkat T cells. Upon contact with the substrate the hybrid vesicles rupture to form the nSLB. By using this experimental protocol naturally occurring cell membrane components, such as membrane proteins, can be transferred to the bilayer. Formation of the hybrid vesicles is done through bath sonication to fuse *synthetic vesicles* and *native membrane vesicles (NMVs).* First, the most optimal sonication parameters to ensure a good mixing of the two types of vesicles was evaluated. It was found that sonicating at 35°C 45 min gave a good mixing of NMVs and synthetic vesicles. These hybrid vesicles were next used to form the nSLB, which was characterized in detail. The diffusivity of lipids in the nSLB was measured using fluorescence recovery after photobleaching and found to be 1.00 $\mu m^2/s$. This was 16 % lower compared to a similar SLB without native material and similar to the diffusivity measured by others for nSLBs, indicating that an nSLB has formed. The immobile fraction of lipids was 21% for the nSLB which was significantly higher than the 5% measures for an SLB without native material. This could be due to unruptured vesicles, which could also be observed in the fluorescence microscopy images. Antibodies targeted at different T-cell proteins were finally used to investigate how well these proteins had been incorporated in the nSLB and whether they were mobile. Both the proteins CD45 and TCR could be detected at a surface concentration < 100 molecules/μm^2 in this way. However, essentially all of the antibodies were immobile on the nSLB, which could be due to the proteins interacting with the underlying support or being confined to vesicles. This needs to be taken into consideration if using this as a model membrane system for T cells, but for experiments where the mobility is not of primary concern then the developed nSLB could make it possible to study the interaction with T-cell membrane proteins under more controlled conditions.

Nomenclatures and abbreviations

SLB – Supported Lipid Bilayers.

Vesicle - A structure comprised of a lipid bilayer enclosing a volume of fluid.

PEG – Polyethylene Glycol

POPC - 1-palmitoyl-2-oleoyl-sn-glycero-3-phosphocholine

HEPES - 2-[4-(2-hydroxyethyl)piperazin-1-yl]ethanesulfonic acid

Synthetic vesicles – Vesicles composed of synthetic vesicles. In this work, synthetic vesicles refers to vesicles comprised of PEG5000-ceramide and POPC.

NMV – Native Membrane Vesicles. These vesicles contain native cell membrane components.

Hybrid vesicles – Vesicles that contain synthetic lipids, as well as native cell membrane components.

FRET – Förster Resonance Energy Transfer.

TIRFM – Total Internal Reflection Fluorescence Microscopy.

FRAP – Fluorescence Recovery After Photobleaching.

Sonication – Applying sound waves to agitate particles in a sample.

T cells – Immune which play a prominent role in the adaptive immune response.

APCs – Antigen Presenting Cells.

Table of contents

1. Introduction

The cell membrane is a biological membrane consisting of a lipid bilayer with proteins embedded in it. It is able to compartmentalize many of the chemical reactions in the cell and protect the cell from its surroundings while also being able to facilitate cell-cell communication and regulate the transportation of certain chemical species across the membrane. Due to its many roles in cellular communication, the importance of studying biological membranes cannot be understated. Particularly in the field of immunology where the proper immune response to the exposure of pathogen is dependent on the communication between cells in the immune system, which occurs via the cell membranes and the membrane proteins that are embedded in them.

As much as cell membranes and membrane proteins are responsible for maintaining a functional immune system, compromised cell membranes and proteins often play major roles in life-threatening disorders. A few examples of disorders, which are characterized by disrupted cell membranes, or malfunctioning membrane proteins, are Alzheimer's disease and cystic fibrosis (1). The importance of studying the cell membrane and its embedded proteins is further emphasized by an estimation that approximately 60 % of all drug targets are located on the cell membrane (2).

Traditionally, these studies have required the use of live cells, and live-cell imaging have been a prominent analytical tool in the field of cell biology. However, live-cell imaging often involves placing the cells in conditions which could compromise the health of the cells. For example, consideration has to be taken into how the cellular environment in the culture is maintained and the choice of imaging chamber. In addition, live cells are often prone to photodamage due to the production of free radicals from oxygen (3). Instead, model membrane systems have been developed in an attempt to mimic the cell membrane. But due to the complexity of a live cell membrane, the model membrane system aims to simplify the system so that the effects and properties of individual components in the cell membrane can be highlighted. The lipid bilayer structure is still retained in a model membrane system (4).

One popular model membrane system is the supported lipid bilayer (SLB). The SLB is a planar lipid bilayer resting on a substrate (e.g. glass or mica), separated by a thin hydration layer. Its constituents are often synthetic lipids such as POPC or POPS. The lipid mobility is preserved in the SLB, meaning the lipids can diffuse in the planar bilayer (5). The introduction of the SLB is often attributed to the research conducted by McConnell in the 1980's (6). SLBs have since been widely employed in the study of cell membranes and they are commonly formed using the method of *vesicle rupture*. In this method vesicles are deposited onto a substrate, whereupon the vesicles will adsorb and spontaneously rupture to form a SLB.

Over the years since, there has been an increase in the interest of using SLBs to study cell-cell interactions in the immune system. One example of such a topic, of which this thesis work is related to, is the question of how T-cell signalling is initiated in the immune system. It has been found that certain membrane proteins on the surface of T cells segregate and organize into specific patterns during interactions with other cells. How these patterns are formed and the role that they play in cell-cell communication is not fully understood. SLBs

have been used in recent work to investigate these questions by integrating the pivotal membrane proteins, in T-cell signalling, onto an SLB and then replicating a real cell-cell interaction with a cell to investigate the function of the proteins during the signalling process (7).

In these studies, the SLBs have largely been comprised of synthetic lipids. Furthermore, only the proteins of interest are integrated onto the lipid bilayer. This contrasts with a native cell membrane which contains hundreds of different lipid types and a multitude of integrated membrane proteins (8). Therefore, while the SLB is able to model the cell membrane by having the lipids and proteins retain their mobility in the bilayer, it can be an oversimplified system of a native cell membrane. In addition, each protein has its own protocol for integrating into the lipid bilayer which can turn into a time-consuming, and in other cases an impossible, process. By incorporating naturally occurring cell membrane components into the SLB, the compositional complexity is increased and a closer mimic of the cell membrane can be expected to be produced.

The goal of the thesis was to establish an experimental protocol for the formation of native-like SLBs (nSLB). Specifically, the protocol aims to describe a process of incorporating native cell membrane material from *Jurkat T cells* into an artificial SLB made from synthetic lipids. The experimental protocol is primarily based on the works by Hudson et.al. (9). The resulting bilayer is then observed with fluorescence microscopy. Fluorescently-labelled antibodies specific for certain membrane proteins were then used to verify the presence of native membrane components in the nSLB. Furthermore, to characterize the newly formed nSLB the diffusion constant was measured for the lipids in the bilayer as well as for the proteins. In short, a method for forming nSLBs out of Jurkat T cells was established and optimized here at Lund University. The resulting bilayer could in principle be used as a more accurate model membrane system for the study of immune-cell interactions.

2. Theoretical background

2.1. The cell membrane

The basic building block of a cell membrane is the lipid. Lipids have an amphiphilic nature, meaning the molecule has one hydrophilic region and one lipophilic region. When subjected to a polar solvent, such as water, the lipids start to reconfigure themselves to form the most energetically favourable structure. Driven by the hydrophobic force, the lipids form a *bilayer* where the hydrophilic parts of the lipids are oriented towards the polar the solvent while the lipophilic parts are interacting with each other. This way, the contact area between the lipophilic regions of the lipids and the polar solvent is minimized (10).

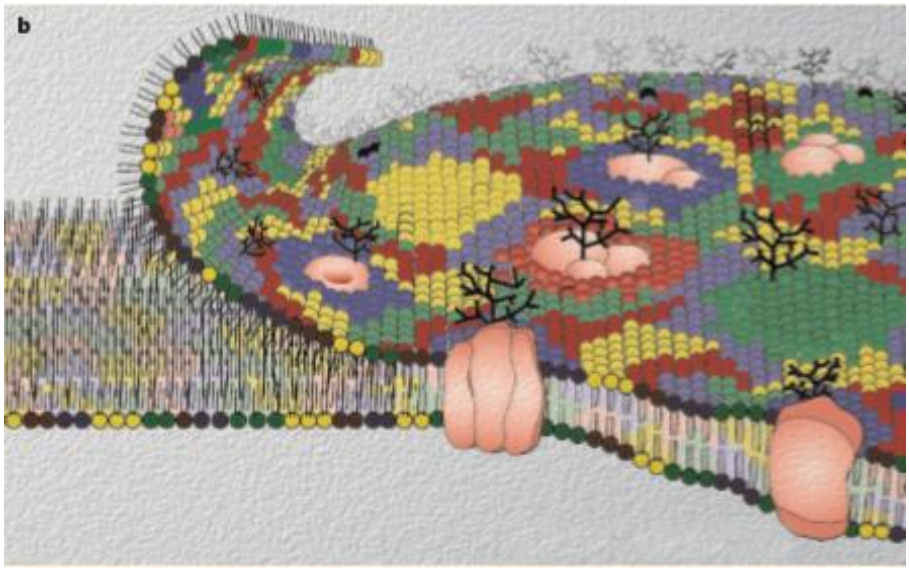

Figure 1: An illustration of the cell membrane according to the fluid mosaic model. The bilayer is composed of two lipid layers and the lipid types are color coded (10).

The contents of a cell are enclosed by this bilayer called the *cell membrane*. Cellular components are protected from the surrounding environment while also playing a large part in facilitating the necessary exchange of essential chemical species with the outside environment and signalling processes. To aid in many of these functions, the cell membrane has a variety of proteins integrated into it. According to the fluid mosaic model, as illustrated in figure 1, the cell membrane can be viewed as a two-dimensional viscous fluid where the integrated lipids and proteins are able to diffuse (11).

2.2. The immune system and T cells

As previously mentioned, model membrane systems have been used to study cell-cell interactions in the immune system. The body's immune system is comprised of the *innate immune system* and the *adaptive immune system*. The two parts are differentiated by the specificity in the response towards the exposure of a pathogen. In regard to the innate immune system, physical barriers (such as the skin) and chemical barriers (such as the acidity of the stomach) are often included and viewed as the first line of defence for a pathogen. On a more microscopic level the innate immune system also includes certain white blood cells (such as the *neutrophils, macrophages and monocytes*) that are able to recognize pathogens based on structures, called pathogen-associated molecular patterns (PAMPs), that are common among pathogens and microbes. Upon recognition, the white blood cells engulf the detected pathogen, or microbe. The immune response is immediate and is therefore often the first part of the immune system encountered by the pathogen. However, the response is not very specific and is targeted against a general set of PAMPs (12).

In contrast, the adaptive immune response can mount a specific response towards antigens via antigen-specific receptors. But the response takes several days to develop. The adaptive immune system is comprised of *T lymphocytes and B lymphocytes*, and one of the hallmarks of the adaptive immune system is the immunological memory which remembers previously encountered pathogens which results in a faster immune response during a second encounter with the same antigen (12).

Initiating the adaptive immune response relies primarily on the interaction between T cells and antigen-presenting cells (APCs). The antigen, presented by the APC, is attached to a major histocompatibility complex (MHC) on the cell membrane. Upon antigen presentation the MHC binds to a molecular complex called the T cell receptor (TCR) on the T cell. If the TCR recognizes the antigen, the T cell is *triggered.* This furthers the development of the adaptive immune response by for example releasing cytokines causing nearby immune cells to proliferate and differentiate into cells with the right functionality to combat the pathogen (12).

Antigen recognition by the T cell is not solely determined by the TCR and MHC. Several membrane proteins are involved in facilitating an optimal interface between the two cells. Close contact areas need to form between a T cell and an APC for the TCR and MHC to efficiently bind. For these purposes the T cell have *adhesion molecules* on its surface that bind to membrane proteins on the surface of APCs. An example of this is *CD2 and LFA-1*, present in the cell membranes of T cells, which bind to CD58, and ICAM-1 respectively, on APCs (13). In addition, the TCR triggering is accompanied with intracellular residues on the TCR becoming phosphorylated by a kinase called *Lck*. This phosphorylation is regulated by the phosphatase *CD45* which removes a phosphate group from the TCR, thus keeping it idle (7). Figure 2 depicts a close contact area between a T cell and an APC along with many of the previously mentioned membrane proteins.

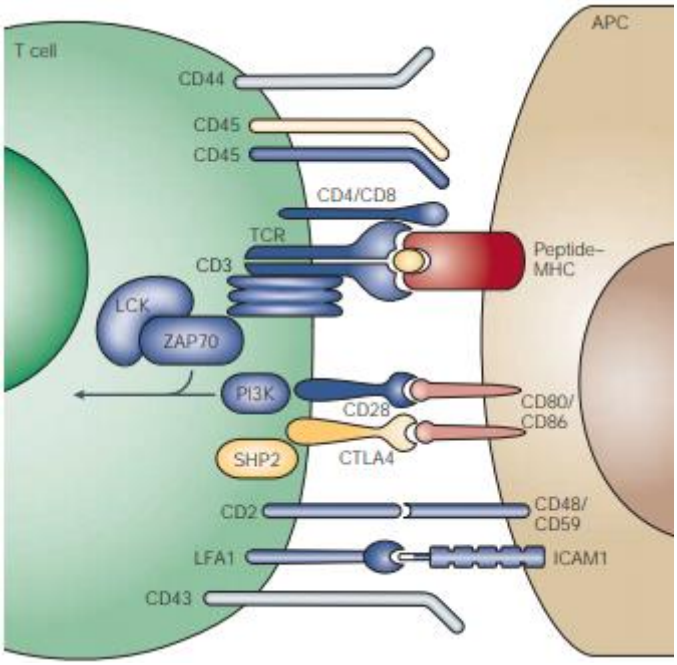

Figure 2: An illustration of a close contact area between a T cell and an APC. The essential membrane proteins taking part in forming the close contact area is also depicted (14).

The distribution of the abovementioned membrane proteins in a T cell membrane have been shown to vary at different stages of T-cell triggering. How the molecular mechanism behind the triggering is affected by the distribution of these proteins still require further studies to gain a better understanding of the interactions between T cells and APCs (7). However, due to the complexity of the cells, in vivo studies of the molecular mechanisms have not been very practical. Furthermore, the shape and morphology of the cell is always changing during

handling which may affect the interaction between two membrane receptors and does not contribute to a controlled experimental environment.

Instead SLBs are used for *in vitro* studies to study the beforementioned research questions. In this work, the native T cell membrane components will be derived from *Jurkat T cells*, an immortalized cell line of a T lymphocyte often used in studies of T-cell signalling (15).

2.3. Supported lipid bilayers

The SLBs, that are used in these *in vitro* experiments, mimics the lipid bilayer of native cell membranes and is supported by a substrate underneath, thus giving high stability. This allows for the bilayer to stay largely intact during handling and these systems are even suitable for experiments running over long periods of time. In addition, the dimensions of the SLB can be large as on the centimeter scale which is considerably larger than the surface dimensions of a generic T cell. This allows for examination of the cellular interactions of multiple cells at the same time.

The experimental protocol presented in this work can be seen as a *top-down approach*, where a larger structure is formed (most commonly a vesicle or liposome) and collapses to form a bilayer with the same lipid composition and protein content as the precursor.

The top-down approach that is adopted in this experimental protocol involves the *adsorption* and *rupturing* of vesicles. The method is considered a more versatile method for forming SLBs and does not require overly expensive equipment (9).

Before expanding on the theory behind the formation of nSLBs, a short description of how a *traditional* SLB (defined as a lipid bilayer formed out of synthetic membrane components) is formed from vesicles is presented below.

2.4. SLB formation

A common method for SLB formation centers around *vesicle rupture*. The lipid composition of the SLB, that is formed from this process, is dependent on the lipid composition in the vesicles.

Vesicles are formed by having the lipids, that will constitute the bilayer, put in a buffer solution. At this stage multilamellar vesicles can form but to obtain unilamellar vesicles, the sample is subjected to ultrasound to agitate the vesicles. The vesicles are then deposited onto a substrate, which is most commonly glass as it will be in this work. The vesicles *adsorb* when they come in contact with the surface of the glass. The adsorption of vesicles to the surface is affected by electrostatic forces and the properties of the substrate will therefore have to be considered (5,16). The glass slides, that are used in this case, are cleaned with a Piranha solution which is a mixture of sulphuric acid and hydrogen peroxide. This surface treatment removes dirt and organic residues off the surface on the glass slide, in addition to adding -OH groups thus making the surface more hydrophilic and increasing the electrostatic forces between the surface and the vesicles (16).

Upon adsorption the vesicles rupture to form SLB patches due to the stress that arise from the curvature of the bilayer (8). The vesicles rupture at the edge of the vesicle-glass contact area where the deformation is at its largest. Studies have been conducted to investigate the

pathway in which the vesicles rupture. There are multiple rupture pathways, but Reimhult et al. argues that pathway (ii) in figure 3 is the dominant rupturing mechanism. This involves the vesicles rupturing in such a way that the lipids in the outer layer of the vesicle bilayer ends up facing the substrate at the end of the rupturing process (17).

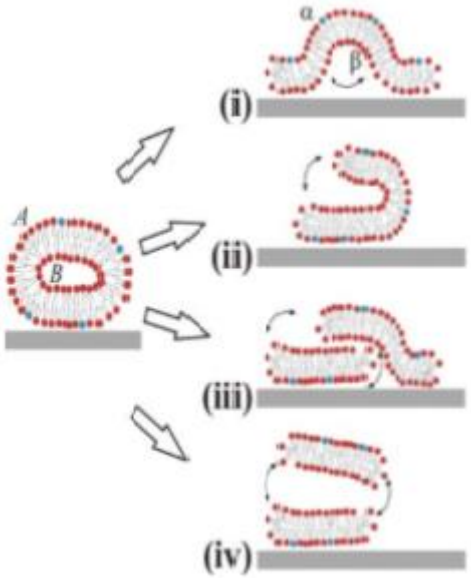

Figure 3: An illustration of four possible rupturing pathways. In pathway (i), the vesicle ruptures in such a way that the outer monolayer of the vesicle is facing the bulk solution. In (ii) the vesicle ruptures at a point of high membrane curvature and unfolds to expose the inner monolayer to the bulk solution. In pathway (iii) the vesicle is divided into two halves where one half adsorbs to the substrate next to the other half in such a way that 50 % of all the lipids in each respective monolayer is exposed to the bulk solution, and the other 50 % is exposed to the substrate. In (iv) the vesicle divides into two halves but one half desorbs from the other half. Pathway (ii) is the dominant pathway for most rupturing events (17).

In addition, the process is also size-dependent. Smaller vesicles have a higher membrane curvature and thus have a higher tension over the surface area, as compared to larger vesicles. Smaller vesicles are thus more inclined to rupture (18). The vesicles that have been described so far in the process are of various sizes. But to ensure that smaller vesicles are used in the formation of a SLB, the sample containing the vesicles are subjected to sonication. Here, sound of ultrasonic frequency is applied to the sample to disrupt larger vesicles into smaller ones. Further details about this process can be found in section 3.2.

Despite all of this, rupturing of isolated vesicles on the glass surface is quite rare (19). Instead, the rupturing of a vesicle to produce a SLB patch is largely affected by its neighbouring vesicles. SLB patches are formed after the rupture of a few vesicles and as patches of SLBs are formed, the edges of the bilayer patches are exposed to the substrate and the bulk solution. The bilayer edges are highly energetic and are able to promote vesicle rupture in adjacent vesicles. The vesicles have a higher affinity for the bilayer edges than the substrate and as more and more SLB patches are created, so does the number of bilayer edges. Aside from increasing vesicle adsorption, the bilayer edges also catalyse a string of rupturing event that results in the formation of multiple SLB patches. To decrease their edge length (which are energetically unfavourable), adjacent SLB patches coalesce to form a complete SLB (5). Vesicles have a lower affinity for the SLB than for the substrate, further vesicles adsorption and rupturing will therefore not occur to a larger extent (8).

Furthermore, the decreasing number of SLB edges also results in fewer vesicles adsorbing to the surface (19). In this regard, it is essential that the concentration of adsorbed vesicles on the surface is above a certain *critical concentration*. At this concentration, the bilayer edges are in close enough proximity to coalesce, and to nearby adsorbed vesicles to promote rupturing processes (5).

One challenge, or limitation, to the traditional SLB has always been the difficulty of incorporating transmembrane proteins into the bilayer. Early attempts to do so resulted in the measured mobility of the proteins in the bilayer, to be significantly lower (or even immobile) compared to the value obtained for free bilayers with the same protein incorporated into it. The given explanation for this issue was unwanted interactions between the transmembrane proteins and the substrate underneath, due to the hydration layer being too thin. Aside from the decreasing mobility issue, the transmembrane proteins could also lose its functionality from interacting too much with the supporting substrate. These types of problems had to be resolved if the SLB was to be used to study how transmembrane proteins behaved in a lipid bilayer. One solution came in the form of using a polymer cushioning technique. One example is lipids conjugated to polyethylene glycol, *PEG*, would be incorporated into the bilayer as shown in figure 4.

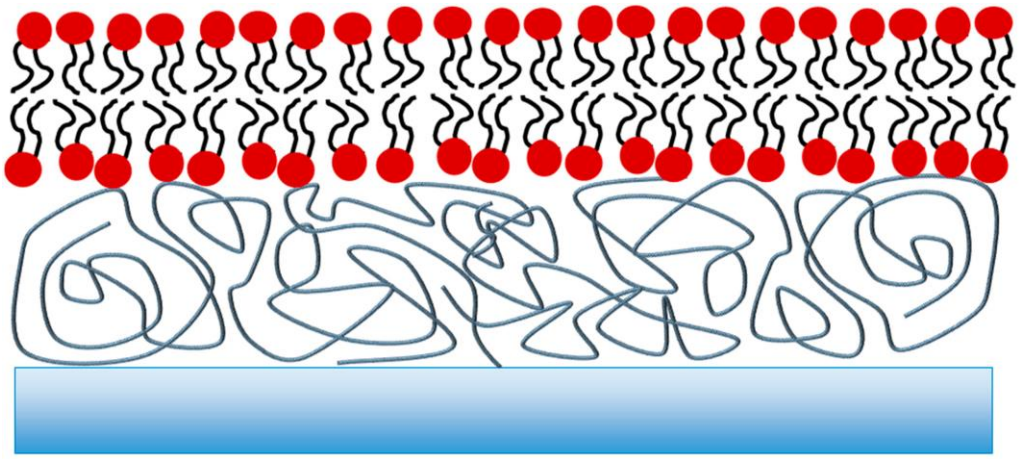

Figure 4: A cross-section view of a SLB containing PEG-ylated lipids. The bilayer is made from synthetic lipids which rests on a substrate (bottom blue structure). A fraction of the lipids is conjugated to polyethylene glycol, PEG, (illustrated by the line drawing structures between the bilayer and substrate) a large molecular structure which elevates the bilayer further above the substrate via spatial displacement (20).

This is done by incorporating PEG-ylated lipids into the vesicles, used for forming SLBs. The result is the SLB being further raised above the substrate which decreases the coupling between the proteins and the substrate (21).

2.5. Formation of native-supported lipid bilayers (nSLB)

Native cell membranes have a higher degree of complexity in terms of its lipid composition and protein content, a complexity which the traditional SLBs do not match. In this type of research, a SLB closer in resemblance to native cell membranes would therefore be a better tool for studying cell-cell interactions and the results would yield a better estimate of the molecular interactions between the T cells and APCs. The goal of this thesis is to form such native-like SLBs and to do that, the work have focused on modifying the protocol of making

nSLBs by Pace et al. (9). The study by Pace et al. centers around the integration of native cell membrane components from the insect cell line *Spodoptera frugiperda*, rather than Jurkat T cells. As a consequence, the experimental protocol had to be adapted and modified for the integration of Jurkat T cells into SLBs in my MSc project. A brief summary of the work by Pace et al., and their experimental protocol, is given below.

Pace et al. present an experimental protocol to form SLBs, on a glass surface, that contain parts from synthetic vesicles (as in the previous cases) as well as components from *native membrane vesicles*, NMVs (the formation of these vesicles is described in section 5.1.), derived from the insect cell line *Spodoptera frugiperda*. This strategy results in a SLB which still retains the lipid mobility, as well as the membrane proteins present in the native cell membrane. To accomplish this, the SLB is formed by depositing what is called *hybrid vesicles*. The hybrid vesicles contain components from both the synthetic vesicles, as well as the NMVs. Forming the hybrid vesicles is done by placing a sample containing both synthetic vesicles and NMVs, in a bath sonicator where ultrasound is applied to disrupt the vesicles in the sample. When the lipids undergo self-assembly, the resulting vesicle is both bigger than the previous vesicle species as well as containing components from both the synthetic vesicles and NMVs.

A successful sonication (where the majority of synthetic vesicles and NMVs form hybrid vesicles) depends on a variety of parameters. Pace et al. chose to focus on the *volume ratio of synthetic vesicles and NMVs, sonication time and temperature*. The optimal sonication parameters were found using *Förster resonance energy transfer*, *FRET, analysis*. The synthetic vesicles are labelled with pairs of fluorophores. An energy transfer between the fluorophores results in a strong fluorescence of a specific wavelength, which is detected by a fluorophotometer. This energy transfer is heavily depended on the distance between the fluorophores. The hybrid vesicles are bigger than the synthetic vesicles which also results in a bigger surface area. The FRET-fluorophores that are incorporated into the hybrid vesicles, will thus be further apart and the energy transfer will therefore decrease as a result of the two vesicles mixing.

Using the optimal sonication parameters, hybrid vesicles for the formation of nSLBs were formed. The hybrid vesicles are deposited onto a clean glass slides along with fluorescently labelled synthetic vesicles dubbed as *tracer vesicles*. Direct observation of nSLB formation was done through the use of fluorescence microscopy. As the hybrid vesicles rupture, so does the tracer vesicles due to the influence of neighbouring ruptured vesicles described in the previous section. While still a vesicle, the fluorophores are in proximity of each other and the intensity of the fluorescent emission is high. As the vesicles rupture and a SLB is formed, all the lipid components including the fluorophores have a much larger area to move along. The intensity of the fluorescent emission will thus decrease as the fluorophores diffuse away from each other, thus confirming SLB formation. These events are captured by the fluorescence microscope where bright spots on the image disappear over time (interpreted as vesicles rupturing) shown in figure 5 below:

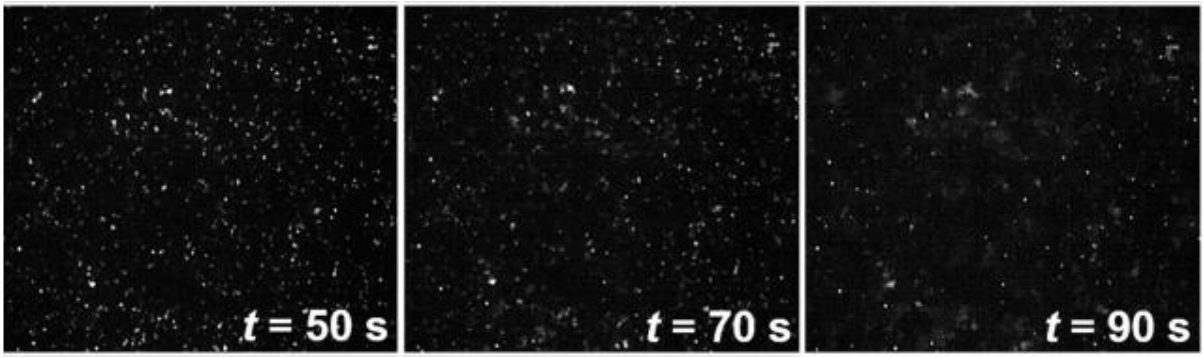

Figure 5: An excerpt from the article by Pace et al., 2015 showing the formation of a hybrid SLB. The hybrid vesicles are deposited onto a substrate along with fluorescently labelled tracer vesicles. The images are taken with Total Internal Fluorescence Microscopy. Vesicles are visible as they adsorb to the surface, which is best represented in the image taken at t=50 s. As time progresses, more vesicles undergo rupturing events as shown in the remaining images as they are darker (9).

Characterization of the bilayer was done using fluorescence recovery after photobleaching, *FRAP*. The light in the microscope is focused to a small region of the sample, resulting in a region of bleached fluorophores which appear on the microscopy image as a black spot. Given that the fluorophores are conjugated to lipids and are able to diffuse freely around in the bilayer, the bleached spot regains its initial intensity over time. The recovery time depends on the diffusion constant of the lipids in the nSLB, thus allowing the authors to calculate the diffusion constant in the bilayer. While the use of tracer vesicles was an indirect method of investigating the rupturing of hybrid vesicles, a more direct confirmation was made by using a fluorescently labelled peptide inhibitor for *BACE1*. BACE1 is a transmembrane protease, playing a part in the formation of myelin sheaths (22) which is found in the particular NMVs used by the authors. The binding of the peptide inhibitor was observed in a fluorescence microscope and furthermore, a diffusion constant of BACE1 could be calculated using FRAP. This confirmed the presence and successful integration of NMV material into the bilayer. A summary of the formation process is illustrated in figure 6.

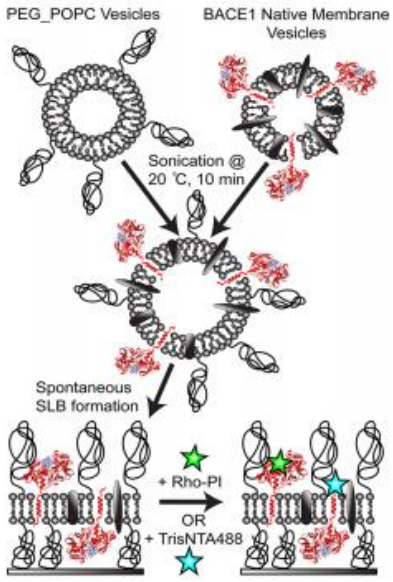

Figure 6: A summarizing graph of the experimental protocol for the formation of a nSLB, as described in the article by Pace et al., 2015. NMVs are first mixed with synthetic vesicles which are sonicated at an optimal sonication setting (the optimal sonication parameters for the work described in the article, are shown in the figure as "20˚C 10min"), to form hybrid

vesicles. The hybrid vesicles are deposited onto a glass slide where the vesicles spontaneously rupture to form a continuous nSLB. To measure the mobility of the lipids and integrated membrane proteins, the bilayer is labelled with fluorescent markers(Rho-PI and TrisNTA488) as illustrated by the coloured stars (9).

3. Experimental background

3.1. Förster Resonance Energy Transfer (FRET)

Many biological processes depend on the interaction between proteins. One way to visualize the proteins in a sample to determine whether they ever come in proximity of each other, is to use fluorescence microscopy. The proteins of interest are tagged with a fluorophore that absorbs light of a specific wavelength, and emits light at a longer wavelength. The emitted light is then collected to construct a picture where the position of the protein is visualized. However, the resolution in a microscope is determined by the expression (23):

$$Resolution = \frac{\lambda}{2 \cdot NA} \quad [1]$$

Where λ is the wavelength in the light and NA is the numerical aperture, which is a measure of how much light an objective can gather. For a common microscope objective of 60x magnification, the resolution is approximately 0,29 µm (23). Unfortunately, the size of an average protein and the distance at which they interact over is a hundred times smaller than the length scales resolvable by a common fluorescence microscope. *Förster resonance energy transfer* (FRET) is a technique able to overcome these resolution limitations. FRET is applicable to studying interactions between proteins when the distance between the fluorophores, that are attached to the proteins of interest, are 10 nm or less (24).

The technique is based on the usage of two fluorophores. One is dubbed the *donor* fluorophore and the other the *acceptor* fluorophore and they have an overlapping absorption and emission spectra as exemplified in figure 7.

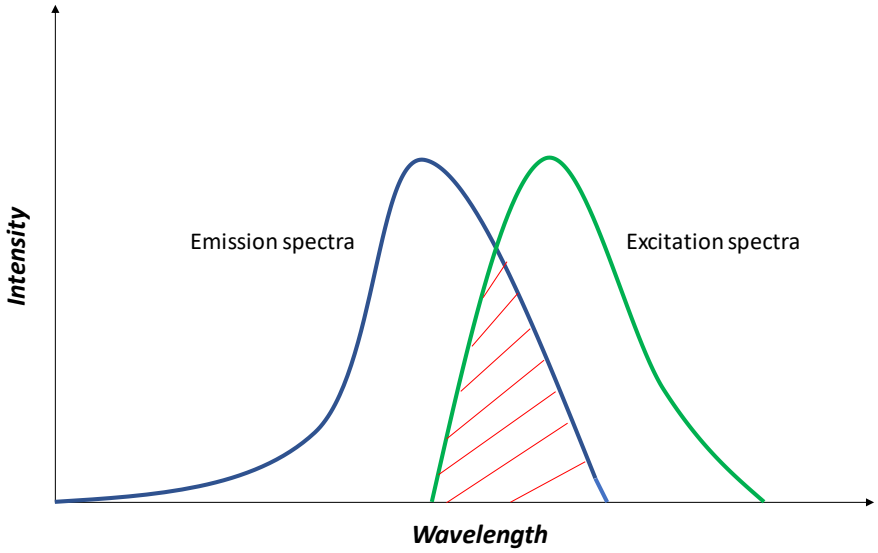

Figure 7: A general graph showing the emission spectra of a donor fluorophore (blue line) and the excitation spectra from an acceptor fluorophore (green line). The overlapping region between the two spectra is highlighted with red lines. An overlapping region indicates the two fluorophores are able to undergo an energy exchange at sufficiently small distances.

To employ the FRET technique a laser of a specific wavelength excites the donor fluorophore, at which point the molecule will start to behave like an *oscillating dipole* with a certain resonance frequency. An energy exchange is able to take place between the donor- and acceptor fluorophore if the acceptor fluorophore has a similar resonance frequency. As a result of the energy transfer the acceptor fluorophore is able to undergo an emission similar to its own inherent emission spectra. The energy transfer is depended on the distance between the two fluorophores, and is expressed as (24):

$$E = \frac{1}{1 + \left(\frac{r}{R_0}\right)^6} \quad [2]$$

Where r is the distance between the two fluorophores and R_0 is the *Förster distance*, where the energy transfer between the two fluorophores is 50 %. The energy transfer is thus very sensitive to the distance between the fluorophore pair due to the factor r being raised to the power of six and can therefore act as an indicator of the distance between them. The R_0-value is determined separately for each fluorophore pair and is done so by (24):

$$R_0 = \left(2.8 \cdot 10^{17} \cdot K^2 \cdot Q_D \cdot E_A \cdot J(\lambda)\right)^{1/6} nm \quad [3]$$

Where K^2 is the *orientation factor* (governed by the angles between the two fluorophores and is often given the value of two thirds) between the donor and acceptor fluorophores, Q_D is the *quantum yield* for the donor and E_A is the *extinction coefficient* for the acceptor. $J(\lambda)$ is the overlap integral and represents the region of overlap between the absorption spectra of the donor fluorophore, and the emission spectra of the acceptor fluorophore. It is illustrated as the hatched region in figure 7. The R_0- value is~~,~~ typically on the order of~~,~~ 5 nm (24).

In the context of this thesis, the FRET technique is used to verify the mixing of synthetic vesicles and NMVs has occurred to form hybrid vesicles. Synthetic vesicles are tagged with pairs of fluorophores which can undergo FRET (as described above) at close distances. During the formation of hybrid vesicles, lipids and membrane proteins from the NMVs are incorporated into the synthetic vesicles. As illustrated in figure 8 this incorporation results in a bigger vesicle and as a consequence, a larger intermolecular distance between the pairs of fluorophores (9).

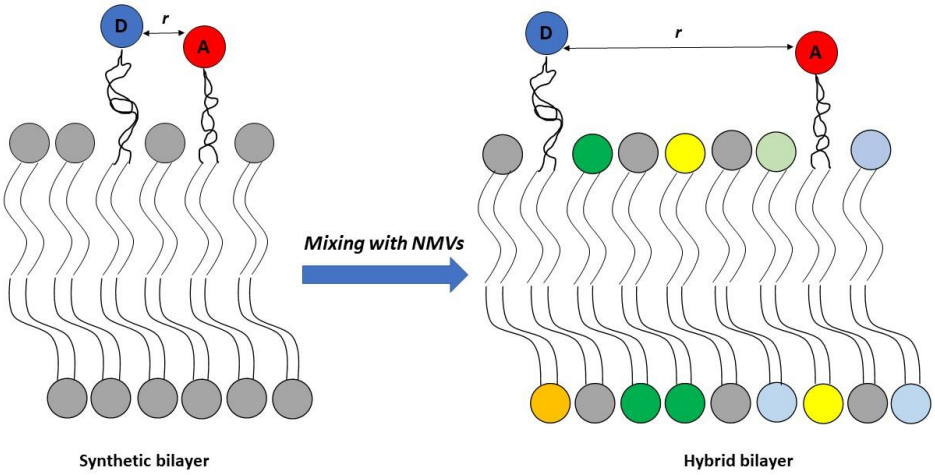

Figure 8: An illustration of how the FRET technique is used as an indication of a successful mixing between two vesicle types. Prior to the mixing with NMVs, the synthetic bilayer (which forms the vesicle) is composed of synthetic lipids as shown by the grey lipid heads. The synthetic bilayer is marked with a donor fluorophore (blue circle marked with a D) and an acceptor fluorophore (red circle marked with an A), separated by a distance r. When mixing with NMVs occurs, native cell membrane components such lipids (as well as membrane proteins, although not shown) are integrated into the bilayer. These lipids are shown as multicoloured in the figure. The integration of these lipids results in a hybrid bilayer and the lipids from the NMVs separates the donor and acceptor fluorophore further. The increasing distance results in a lower energy exchange as described by equation [2].

According to equation [2], the mixing of the two types of vesicles would result in a lower energy transfer which is detectable using a spectrophotometer.

3.2. Sonication

The mixing of NMVs and synthetic vesicles, to produce hybrid vesicles, is done through bath sonication.

In this technique a vesicle sample is placed in a bath whereupon sound waves with ultrasonic frequencies will be applied. However, it is not clear as to how this step in the process leads to the formation of hybrid vesicles that are larger in size compared to the two constituent vesicles. One possible pathway could be that the application of ultrasounds provides the vesicles with enough energy to overcome an energy barrier to eventually fuse together.

As previously mentioned the FRET technique is utilized, by tagging the synthetic vesicles with pairs of fluorophores, as an indicator of how well the NMVs merges with the synthetic vesicles. The *temperature* in the bath sonicator, as well as the *sonication time*, are two crucial sonication parameters that affects the vesicle mixing. Increasing the sonication time exposes the vesicles to the sound waves for a longer period of time, resulting in a larger fraction of vesicles being disrupted as well as producing smaller vesicles. Increasing the temperature leads to an increase in membrane fluidity, making them easier to deform (25). It should however be stated that the sonication parameters which leads to maximum amount of NMV incorporation is not always regarded as the optimal sonication parameters. Incorporation of native cell membrane material also includes membrane proteins. Since the functionality of the nSLB is largely depended on the membrane proteins that inhabit it, the effect that the sonication exerts on the membrane proteins have to be considered. The

Jurkat T cells in this work are cultivated at 37˚C. Sonication at a temperature above this temperature risks denaturing the proteins. Furthermore, sonication is a vigorous process and prolonged sonication can damage the proteins (26).

Optimal mixing in this case refers to the maximal amount of mixing without sacrificing the quality of the membrane proteins.

3.3. Fluorescence Microscopy

Hybrid vesicles that will spontaneously form a SLB will be formed using the identified optimal sonication parameters. The nSLB will be observed using *Fluorescence microscopy.* As the name suggests, the technique is based on fluorescence whereby certain molecules are able to absorb light of a specific wavelength and then emit energy at a longer wavelength. The technique has been widely employed in biological research and it is done by tagging the, for example, cells and proteins of interest with fluorophores. The process can be described as follows; a laser shines on the sample with light of a wavelength corresponding to high absorption among the fluorophores. Upon excitation, electrons will move from a ground state to an excitation state. Due to energy loss from vibrations, the electrons will move to a lower energy state. In the transition back to the ground state, a photon will be emitted with an energy corresponding to the energy difference between the two electronic states the electrons transitioned between. As a result of the energy loss, the light in the fluorescent emission has a longer wavelength compared to the excitation light. The difference is called a *Stokes' shift* and it allows one to separate the excitation light from the sample's fluorescent emission (27). Due to varying brightness in the emissions, the two wavelengths have to be separated so as to not limit the detection. This is solved by placing a dichromatic mirror and emission filters in the microscope to reflect light below a certain wavelength and transmit light above the same threshold (28).

3.3.1. Total Internal Reflection Fluorescence Microscopy (TIRF)

However, a common issue with fluorescence microscopy has been a low signal-to-noise ratio. This arises due to the difficulties in limiting the background noise which can be contributed by fluorophores in the bulk solution. A low signal-to-noise ratio leads to low resolution and overall lower image quality (28).

The principle behind *Total Internal Reflection Fluorescence Microscopy* minimizes this problem by having the laser shining on the sample, from underneath, at an angle. The difference in refractive indices as the light passes from glass to the sample container, determines how the light is refracted and reflected. However, at a critical angle, expressed as (29):

$$\theta_{critical} = \arcsin\left(\frac{n_1}{n_2}\right) \quad [4]$$

Where n_1 is the refractive index in the sample and n_2 is the refractive index in the glass, *total internal reflection* occurs where no light passes through the sample. At the point of reflection a small electromagnetic field, called an *evanescent field*, is generated. This field propagates through the sample but its intensity exponentially decays as the evanescent wave moves propagates through the sample as described by (29):

$$I_z = I_0 e^{-z/d} \quad [5]$$

Where z is the depth in the sample, I_0 is the intensity of the evanescent wave at the interface and d is the depth of the evanescent wave as described by (29):

$$d = \frac{\lambda_0}{4\pi\sqrt{n_2^2 \cdot \sin^2\theta - n_1^2}} \quad [6]$$

Where λ_0 is the excitation wavelength. This results in only the fluorophores in the nearby regions of the point of reflection, to undergo excitation. The penetration depth of the evanescent wave is around 100 nm as compared to 500 nm thick image section of confocal microscopy images. In this manner the background noise is minimized as only fluorophores close to the surface undergoes excitation (29).

3.4. Fluorescence Recovery After Photobleaching (FRAP)

One additional issue with fluorescence microscopy is *photobleaching*. Illumination of a fluorophore over a long period of time leads to its electrons being in a high energy state. In this state the fluorophore is highly reactive with nearby oxygen molecules. The interaction produces singlet oxygen which are able to cleave covalent bonds in the fluorophore, changing its structure and making it permanently unable to fluoresce. However, some techniques have exploited this feature as in the case of *FRAP* which uses this phenomenon to calculate the diffusion constant of the bleached fluorophores. An illustration of the FRAP procedure is shown in figure 9. Fluorophores, conjugated to lipids, in a circular region is bleached as shown in the first image. As time progresses lipids diffuse in and out of the bleached region. Over time, a homogenous concentration of bleached lipids is reached and the intensity of the bleached region moves towards its initial intensity. The time for this recovery to take place is governed by the diffusion constant for the lipids in the bilayer.

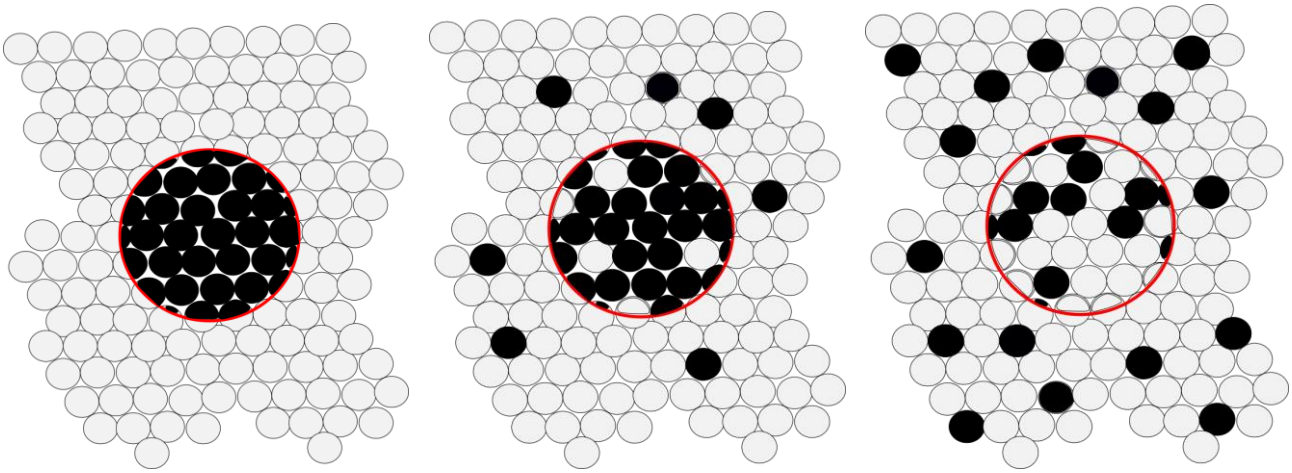

Figure 9: An illustration of a SLB, viewed from the top, during a FRAP procedure at three different time points where $t_1<t_2<t_3$. The bilayer is labelled with fluorescent dyes and each circle represents the head group of a lipid. In the first step ($t = t_1$) the intensity of the light source is focused onto a small region of the SLB. As a consequence, the lipids in the region become bleached as symbolized by the black circles. As time progresses, the bleached lipids diffuse out of the bleached area and unbleached lipids diffuse into the bleached area. As a result, the bleached region is slowly recovering its initial intensity.

By measuring how the intensity in the bleached region changes over time, information of the diffusion constant can therefore be extrapolated. Moreover, by measuring how much of the initial intensity is recovered one can calculate how large the fraction of immobile lipids is via (30):

$$F_{immobile} = \frac{I(t) - I_i}{I_0 - I_i} \quad [7]$$

Where $I(t)$ is the intensity at a given time, I_i is the intensity after the bleaching moment and I_0 is the initial intensity. The intensity is proportional to the amount of fluorophores which makes it possible to calculate the intensity by instead looking at how the concentration of fluorophores change over time. This can be described by Fick's second law:

$$\frac{\partial c}{\partial t} = D\left(\frac{\partial^2 c}{\partial x^2} + \frac{\partial^2 c}{\partial y^2}\right) \quad [8]$$

Where $c(x, t)$ is the concentration of fluorophores and D is the diffusion constant.

The mobility of the bilayer, given by the FRAP measurement, can be affected by unruptured vesicles. To investigate whether any vesicles remain unruptured, the bilayer is labelled with DiD (ThermoFisher), a red fluorescent lipophilic dye. DiD-labelled lipids that are integrated into the bilayer are able to diffuse in the lipid bilayer and will thus only appear with a weak intensity. Any labelled lipids that are part of unruptured vesicles are still confined and will therefore appear as bright spots with high intensity.

4. Goal of the thesis

The aim of the thesis is to integrate native cell membrane material from Jurkat T cells into SLBs normally made from synthetic lipids, thus forming a model membrane system more closely resembling a native cell membrane. This native supported lipid bilayer, nSLB will be formed through deposition of *hybrid vesicles* on a glass surface cleaned with Piranha solution. The hybrid vesicles will be formed by merging synthetic vesicles (comprised of PEG and POPC), with native membrane vesicles, NMVs, containing Jurkat T cell components by the means of sonication. The NMVs were prepared and kindly provided by Marta Bally's group in Chalmers University.

The *first* goal was to find the optimal sonication parameters for the formation of hybrid vesicles, which was evaluated with FRET.

The optimal sonication parameters was used to form hybrid vesicles that spontaneously rupture to form the nSLB. The *second* goal was to characterize the bilayer to detect the presence and mobility of different membrane proteins native to the Jurkat T cells.

4.1. Parameters of interest

Sonication parameters were be comprised of, as it is in the study by Pace et al., water temperature and sonication time. The optimal parameters were judged by the ratio between the acceptor peak, and the donor peak in the FRET technique (the mechanism behind the FRET technique is described in section 3.1). This ratio will henceforth be noted as the *FRET ratio*. As previously mentioned, the health of the membrane proteins should not be

compromised by the sonication process. Not every type of membrane protein can be checked and thus an indicator of membrane protein health was needed. One such indicator is to the functionality of the acceptor fluorophore by using the corresponding excitation wavelength and measuring the fluorescent emission, *before and after* sonication. Similar intensity values in the emission after sonication, as compared with the value before, was interpreted as the acceptor fluorophores not being overly compromised by the sonication process. The health of the acceptor fluorophores acted as an indicator of the effect that the sonication process has on the membrane proteins in the NMVs. This indicator was used in conjunction with the test of applying antibodies to observe whether the membrane proteins are able to bind to the antibodies after sonication.

Characterization of the nSLB was done by measuring the diffusion constant of the lipids in the bilayer and compared with prior known diffusion constants in SLBs solely made from synthetic lipids. The task at hand was made possible by integrating lipids which are conjugated to a fluorescent dye, into the bilayer. A FRAP analysis was then be performed on the bilayer as described in section 3.4.

Secondly, the presence of membrane proteins that are native to the Jurkat T cells was investigated. Six membrane proteins will be of interest and are summarized in table 1:

Table 1: The membrane proteins of interest is summarized along their function in relation to this project.

Membrane protein	**Function**
CD2	An adhesive molecule which bind to CD58 on APCs (13).
CD45	A phosphatase, removes phosphate group from Lck to inhibit TCR triggering (7).
CD18	A membrane protein part of the adhesion molecule LFA-1 that binds to ICAM-1 (31).
MHC	A class of membrane protein present on all cells expect for red blood cells that is responsible for presenting antigens to cells in the immune system (12).
CD4	A coreceptor to TCR (7).
TCR	T cell receptors. Binds to MHC in an APC which results in T cell triggering (12).

Their presence serves as a direct confirmation of a successful integration of NMV material into the SLB. This is done by using antibodies specific for the membrane proteins. In addition, the antibodies are conjugated to a fluorescent dye which allows the binding of the antibodies to the proteins to be visualized using a TIRF microscope, as well as perform a FRAP measurement to measure the diffusion constant of the proteins on the bilayer. These values can then be compared to the diffusion constants of these membrane proteins obtained from native Jurkat T cells.

4.2. Scope and limitations

Before proceeding any further, the scope and limitations of the current work in the thesis should be addressed.

Each bath sonicator is different in terms of power and the frequency in the sound waves that are applied to the volume of water. As such, the optimal sonication parameters that are presented in this work should not be viewed as universal. Rather, it should be viewed as optimal given the specific model of the sonicator. Furthermore, all sonication parameters used to gain optimal results are only applicable to the cell line used in this work. A different cell line may require a different set of sonication parameters and may also carry with it other membrane proteins that differ from the ones tested in this work. Nevertheless, the parameter given in this work can be seen as a good starting point when incorporating NMVs from other mammalian cells into SLBs.

5. Materials and Methods

5.1. Vesicle preparation

The NMVs were obtained through the courtesy of *Marta Bally*'s research group of Chalmers University of Technology. The procedure of making NMVs is as follows. The Jurkat T cells are washed with *phosphate buffered saline, PBS*, and a *protease inhibitor cocktail* (Roche Life Science) to preserve the functionality of the proteins during the process of cell lysis. Next, the cells are centrifuged (Hettich Mikro 22R) for *five minutes* under *410 xg*. The supernatant is removed, leaving a pellet on the bottom containing the cell content. The pellet is resuspended in 3 ml PBS buffer solution and then washed three times. Each washing consists of centrifuging for *five minutes at 1000 xg under 4˚C* and resuspension in 3 ml PBS buffer solution.
The cells are then manually disrupted using a Dounce Homogenizer. The resulting solution is centrifuged for *five minutes at 600 xg*. The process is repeated until no pellet could be observed.
All cell components are now present in the lysed cell solution and the sample is centrifuged for *20 minutes at 3500 xg*. The heavier cell components, such as the nuclei and mitochondria, is collected in the pellet while the lighter cell components are present in the supernatant. The supernatant is removed and ultra-centrifuged at *180 000 xg (Optima LE-8k, Beckman Coulter) for 90 minutes under 4˚C.* The membrane components of the Jurkat T cells are now present in the pellet which is collected and resuspended in PBS and 20 % volume glycerol. NMVs are then snap frozen with liquid nitrogen and stored in -80˚C (32).

The synthetic vesicles used in this work have the following composition:

- *99.5 mol% POPC (Avanti Polar Lipids)*
- *0.5 mol% PEG5000-ceramide (Avanti Polar Lipids)*

Vesicles used for FRET analysis (referred to as *FRET vesicles*) are synthetic vesicles tagged with OregonGreen 488-DHPE (ThermoFisher) as a donor fluorophore, which has an excitation maximum at 501 nm and an emission maximum at 526 nm. The corresponding acceptor fluorophore is Atto647-DPPE (Atto-Tec) which has an excitation maximum at 646 nm and an emission maximum at 669 nm. The FRET vesicles have the following composition:

- *98 mol% POPC (Avanti Polar Lipids)*
- *1.5 mol% Atto647-DPPE (Atto-Tec)*
- *0.5 OregonGreen488-DHPE (ThermoFisher)*

A sample vial made of glass is used to contain the vesicles and is cleaned with chloroform. The stock solution for each lipid have a concentration of 10 mg/ml and the desired amount of PEG5000-ceramide and POPC are extracted, from their respective stock solution, according to the composition of the synthetic vesicles. The lipids are dissolved in chloroform. Removal of the chloroform is essential before forming the vesicles and is achieved by evaporation through the use of nitrogen gas until a dry film of lipids was formed on the bottom of the flask. The dried lipids are thereafter dissolved in HEPES buffer (150 mM NaCl and 10 mM HEPES, pH = 7,41) to a final volume of 1 ml. Final vesicle concentration in the sample was 1 mg/ml.

To form SUVs the sample was sonicated using tip sonication (model VCX 130 by Sonics & Materials, Inc.). In this technique a thin titanium rod is immersed into the sample which then vibrates at a high frequency, causing disruption of the larger vesicles to form SUVs.

The sample is sonicated for a total time of 30 minutes with a 55 % amplitude at 10 second pulses followed by 10 seconds of waiting time. During tip sonication the sample is heated up to high temperatures. To prevent any damages to the vesicles, the sample is immersed in an ice bath during the sonication process. The vesicle sample is thereafter stored in 4˚C.

Preparation of the FRET vesicles are done in the same manner resulting in the same final vesicle concentration.

5.2. Cleaning glass slides

Circular glass slides are cleaned using Piranha solution. This solution is formed by taking 1 ml H_2O_2 (30% purity, Honeywell Burdick & Jackson® Inc.) and adding it slowly to 3 ml H_2SO_4 (95-97 % purity, Merck KGaA). The Piranha solution is kept under heating during the whole duration of the cleaning process. Glass slides are then submerged in the solution where they are kept for 30 minutes, after which they are taken out of the Piranha solution and rinsed with deionized water. To dry off the glass slides without directly touching them, nitrogen gas is used to blow off the water that is on the surface. The nSLB will be formed on the glass slide and a silicon well with a diameter of 4.5 mm (Grace Bio-labs, Inc. Press-To-Seal silicon isolators) is attached to the cleaned glass slide to contain the nSLB in a small volume. Finally, the glass slides are placed in a metallic sample holder as a means of keeping the nSLB stationary when looking at it through a microscope.

5.3. Forming hybrid vesicles through sonication and FRET analysis

Unlike the process of forming synthetic vesicles, forming hybrid vesicles makes use of a bath sonicator (model RM 75 UH from Sonorex Technik Bandelin) instead of a tip sonicator. To find the optimal sonication parameters samples were made consisting of:

- *20 µl NMV (unknown concentration)*
- *1 µl FRET vesicles (1 mg/ml)*
- *39 µl HEPES buffer (150 mM NaCl and 10 mM HEPES, pH = 7,41)*

The sonication parameters are tested according to the water temperature in the bath, and the sonication time. Three samples are made for the testing of each set of sonication parameter, which is listed below:

- *30˚C, 45 minutes*
- *30˚C, 60 minutes*
- *35˚C, 45 minutes*
- *35˚C, 60 minutes*

An image of the experimental setup is shown in figure 10.

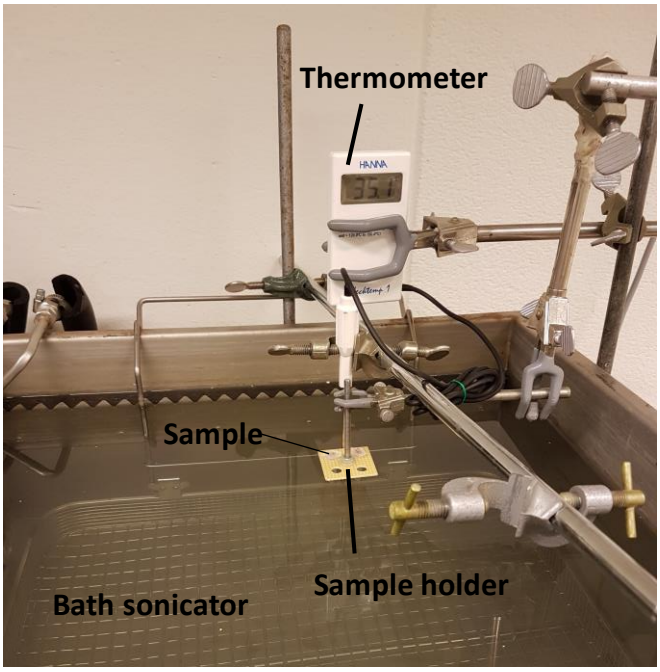

Figure 10: The experimental setup for the sonication procedure. Each sample is put in an Eppendorf tube which is inserted into a plastic holder. A thermometer is placed close to the samples in the holder to measure the local water temperature. The bath sonicator is filled with water to the point where only the sample volume in the Eppendorf tubes are submerged under the water.

A nearby water heater sets the temperature to the desired value and the samples are placed in the center of the bath via a plastic sample holder. A thermometer from Hanna Technologies is placed near the sample holder to monitor the temperature during the sonication process. The temperature rises during sonication due to the application of sound waves. To regulate the temperature and keep it close to the desired temperature, small amounts of ice was added to bath whenever the temperature rose too high. As the sonicator is turned on, disruption to the water surface can be observed. However, the disruption is not equal everywhere on the water surface. Considering three samples are sonicated simultaneously, the platform is rotated at even time intervals to ensure each sample is exposed to the same regions of the water surface during sonication. In addition, the surface disruption is dependent on the water level. As more ice is deposited onto the bath, the water level rises and can be regulated with a valve to draw out excess water.

The results from the sonication is thereafter reviewed in the spectrophotometer (Cary Eclipse Fluorescence Spectrophotometer from Agilent Technologies). Each sample was diluted to 300 µl with HEPES buffer (150 mM NaCl and 10 mM HEPES, pH = 7,41) and transferred to a 500 µl cuvette and inserted into the spectrophotometer. A laser inside the spectrophotometer excites the fluorophores in the sample and measures the intensity of the fluorescent emission as a function of wavelength. The excitation wavelength was set to 488 nm and the fluorescent emission was measured over a range of 498 nm to 750 nm. To complement the result, the functionality of the Atto647-DPPE fluorophores was also examined by changing the excitation wavelength to 645 nm. The FRET ratio was evaluated for each set of sonication parameters to find the optimal ones.

5.4. Forming nSLBs

Samples for the formation of nSLBs were made using the optimal sonication parameters. These samples consisted of 6 µl NMVs and 54 µl PEG_POPC_OregonGreen488-DHPE (1 mg/ml). The concentration of NMVs is unknown but since PEG_POPC_OregonGreen488-DHPE makes up a majority of the sample volume, the final concentration is approximated to also be 1 mg/ml. A picture of a sample in a sample holder is shown in figure 11.

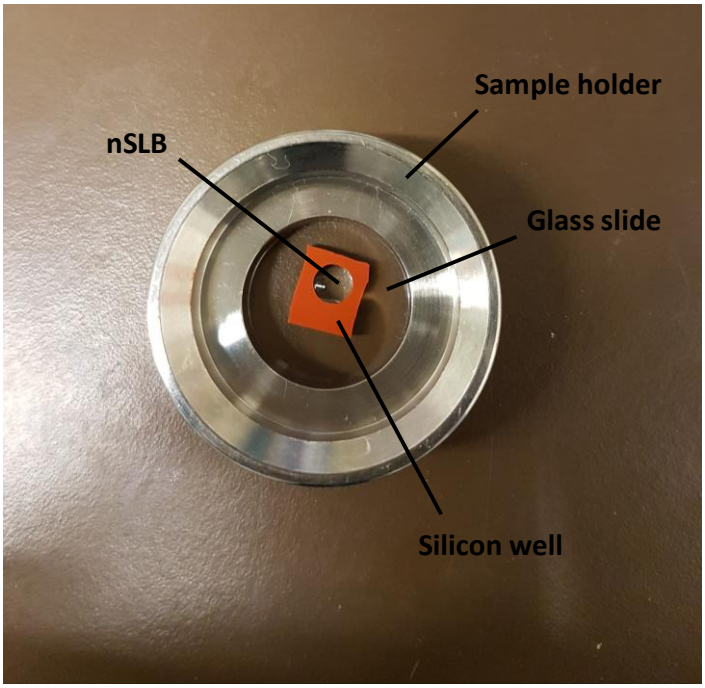

Figure 11: An image of sample used for the formation of a nSLB. A thin glass slide, cleaned with Piranha solution, is placed in a sample holder to weigh it down and aid with the handling of the sample in the microscope. A silicon well is attached to the glass slide and 30 µl of the sonicated sample containing hybrid vesicles are deposited into the well where a nSLB is formed. The nSLB is left to incubate for 1h 15 min.

Based on the work by Pace et al. the sample volume deposited into the well was chosen to correspond to a vesicle concentration of 0.1 mg/ml on the glass surface(9). The silicon well, described in section 5.2, has a volume of 30 µl. 3 µl of the sonicated sample was therefore mixed with 27 µl HEPES buffer and put into the well. The sample was left to incubate for one hour and 20 minutes (during which the bilayer was formed) in the dark so as to not photobleach the fluorophores.

5.5. Characterizing the nSLB and conducting a FRAP analysis

Before examining the nSLB, the well is washed three times with 30 µl HEPES buffer to remove any non-ruptured hybrid vesicles. Removal of these vesicles decreases the amount of background fluorescence when looking at the sample through a fluorescence microscope.

To obtain an image of the nSLB a microscope of the model *Nikon Eclipse TE2000-U* was used. The light source consisted of two lasers (Cobolt AB), one with a wavelength of *488 nm* which is used for the excitation of OregonGreen488, and one with a wavelength of 638 nm used for the excitation of Atto647N. To prevent any excessive photodamage, and photobleaching, to the sample, the light from the laser are passed through a wheel of multiple neutral density filters (Thorlabs). The beam is focused onto the sample and excites the fluorophores by a 60x

oil immersion objective (Nikon). The fluorescent emission is led back through the objective to a sCMOS camera (Hamamatsu Digital) where the image is relayed to a computer screen. The two fluorescent dyes can be studied on two separate channels, where the emission is led through a beamsplitter (Gemini) before reaching the sCMOS camera. Controlling the microscope setting was done using the *Micromanager software* (33) and viewing the images was done with the program *ImageJ*. When viewing the nSLB, the following microscope settings were used:

- *100 ms exposure time*
- *2x2 binning*
- *1.3 ND filter*
- *30 mW for the 488 nm-laser*
- *30 mW for the 638 nm-laser*

To thereafter confirm the presence of a bilayer, a FRAP measurement was conducted. One important note at the start of conducting a FRAP measurement is to adjust the focus to ensure a good image of the bilayer, as well as finding a region which has been exposed as little as possible to the light (to minimize the amount of photobleaching). The FRAP measurement process is managed by a written script in Micromanager. Firstly, a couple of frames of the illuminated area are taken with settings predetermined by the user. At this point a FRAP-lens is manually inserted in the laser beam. Thereafter the ND filters attenuating laser beams are removed, meaning the region of interest is now illuminated at full intensity (60 mW for the 488 nm-laser and 140 mW for the 638 nm-laser). The lens focuses all of the incoming light into a small spot of the illuminated area, causing the fluorophores in that region to photobleach. The bleaching lasts for *three seconds* after which the FRAP-lens is removed and the predetermined ND filter is reinstated. A series of frames are then taken of the illuminated area, showing the bleached spot recovering its initial intensity should a bilayer have been formed. During the FRAP measurement there is a *two-second* interval between each frame.

To investigate whether any vesicles remain unruptured, the bilayer is labelled with DiD-labelling dye. Upon application, the sample is left to incubate for 30 minutes.

Next, the nSLB was examined to see whether any of the membrane proteins characteristic of Jurkat T cells have been integrated into the bilayer. The antibodies of interest are summarized in table 2:

Table 2: A table summarizing the membrane proteins of interest and the corresponding antibody used to detect its presence in the nSLB. The antibodies are also conjugated to a fluorescent dye which is also used in the FRAP measurements.

Membrane protein	Antibody
CD45	HI30 (labelled afterwards with Alexa Fluor® 647) (Biolegend)
CD2	CD2 Monoclonal Antibody (RPA-2.10), FITC (eBioscience™)
CD4	CD4 Monoclonal Antibody (RPA-T4), FITC (eBioscience™)

CD18	CD18 (LFA-1 beta) Monoclonal Antibody (6.7), FITC (eBioscience™)
MHC	HLA-DR/DP/DQ Monoclonal Antibody (WR18), FITC (Invitrogen)
TCR	OKT3 (labelled afterwards with Alexa Fluor 488)

Antibodies for the corresponding protein of interest is added to the silicon well. Depending on its initial concentration, the antibody is diluted with HEPES buffer and 20 µl is then added to the well. Antibodies specific for CD2, CD4, CD18 and MHC are conjugated to Fluorescein isothiocyanate, *FITC* which is excitable with the 488 nm-laser. To gain a visual of the presence of these proteins, the antibodies were therefore added to a non-labelled nSLB. On the other hand, the antibody specific for CD45 is conjugated to Alexa Fluor 647, which is excitable with the 638 nm-laser and can therefore be added to the same previous nSLB containing OregonGreen 488-DHPE. The well had been washed with buffer solution after the incubation which removed the majority of antibodies in the bulk solution which haven't bound to the bilayer. A FRAP was conducted to confirm the presence and mobility of the proteins.

Using the frames captured during the FRAP process, a MATLAB programme written by Jönsson et al. was used to calculate the diffusion constants of the lipids and membrane proteins, as well as the immobile fraction (34). A detailed description of its usage is described in the appendix.

It is also of interest to investigate how much native material from the Jurkat T cells that have actually been incorporated into the SLB. One way to do this is to calculate the molecular density of membrane proteins on the surface of the nSLB. This is done indirectly by calculating the molecular density of antibodies on the surface as well as having the assumption that the membrane proteins are homogenously distributed across the bilayer. The molecular density of a certain protein can be calculated in the following way:

1. Dilute a small volume of antibodies to the point where it is possible to image individual antibodies with the fluorescent microscope.

2. Measure the mean intensity from one antibody and subtract the background intensity. The background intensity varies depending on the position in the image. Subtract with the background intensity from a region near the bright spot of choice. Multiply with the number of pixels comprising the marked region of the antibody. Divide by the power (mW) the laser is operating at. This value gives the number of counts per mW. The choice of ND filter also decreases the read-out intensity via:

$$\frac{I}{I_0} = 10^{-d} \leftrightarrow I_0 = I \cdot 10^{d} \quad [9]$$

Where I is the intensity after the filter, I_0 is the incident intensity and d is the optical density of the filter. Multiply the number of counts per mW, with 10^d to obtain the unfiltered intensity per antibody. Repeat this process for multiple spots to gain a mean value ± one std.

3. Take a picture of the nSLB.

4. Mark an arbitrary region of the picture and measure the size of the region in terms of the area of pixels.

5. Measure the mean intensity of the marked region and subtract the background intensity. The mean intensity is the intensity per pixel. Multiply this value with the total number of pixels making up the region to obtain the total intensity. Divide by the power (mW) the laser is operating at and use equation [9].

6. Divide the total intensity with the intensity in the fluorescent emission from one antibody. The product is the number of fluorescent antibodies in the marked region, which corresponds to the number of membrane proteins in that region.

7. The molecular density can thereafter be obtained by dividing the value from step 5 with the number of pixels in the marked region, or with the area given by a known pixel size.

This can be summarized in the formula [9]:

$$c = \frac{I_{total}}{I_{single\ antibody} \cdot Area\ of\ the\ marked\ region} \quad [10]$$

Where I_{total} is the total intensity in the region of a bilayer obtained from step 5, and $I_{single\ antibody}$ is the intensity from a single antibody obtained from step 2.

6. Results and discussion

6.1. FRET analysis

To investigate the conditions that would lead to a good mixing of NMVs and synthetic vesicles, a FRET analysis was conducted at different sonication parameters as described in section 5.4. By using ice, I was able to keep the temperature at ± 1˚C degree around the desired temperature. To observe the difference produced in the FRET measurement due to sonication, a control sample was made. In figure 12, FRET measurements from three samples *before* sonication is presented. Each sample in the control experiment was comprised of 20 µl NMVs (unknown concentration), 1 µl FRET vesicles (1 mg/ml) and 279 µl HEPES buffer solution.

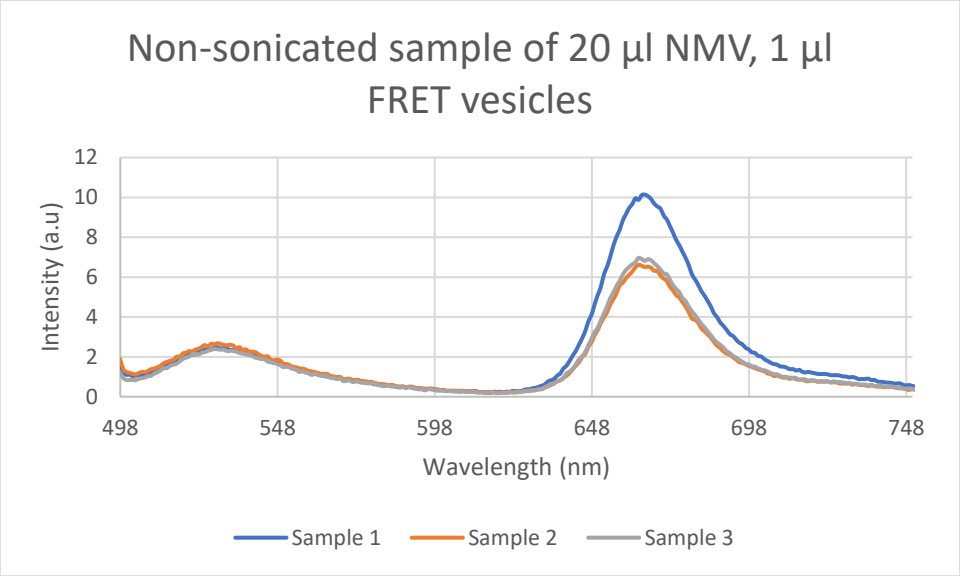

Figure 12: FRET measurements on non-sonicated samples. The sample consisted of 20 µl NMVs, 1 µl FRET vesicles (1 mg/ml) and 279 µl HEPES buffer solution. A smaller donor peak at 526 nm is observable as well as the acceptor peak at 669 nm. The average donor peak value was 2.47 ± 0.11 and the average acceptor peak value was 7.87 ± 1.59.

As shown in figure 12 the acceptor peak is larger than the donor peak despite the excitation wavelength being 488 nm. This is an indication of an energy transfer occurring between OregonGreen488 (the donor fluorophore) and Atto647 (the acceptor fluorophore). A FRET signal is thus produced by the FRET vesicles.

FRET measurements were then made on sonicated samples at different sonication parameters. Three samples, with the same composition as the control samples, were sonicated for each set of sonication parameters and the excitation wavelength was 488 nm. The average results from the FRET measurements for each set of sonication parameters is presented in figure 13.

As the samples are sonicated, the NMVs and the FRET vesicles are fusing together to form hybrid vesicles. This results in the average distance between the donor and acceptor fluorophore to increase. Following from equation [2], this means that the energy transfer between the two fluorophores decreases and more of the donor fluorescent emission is detected by the spectrophotometer, while the emission from the acceptor fluorophore is lower.

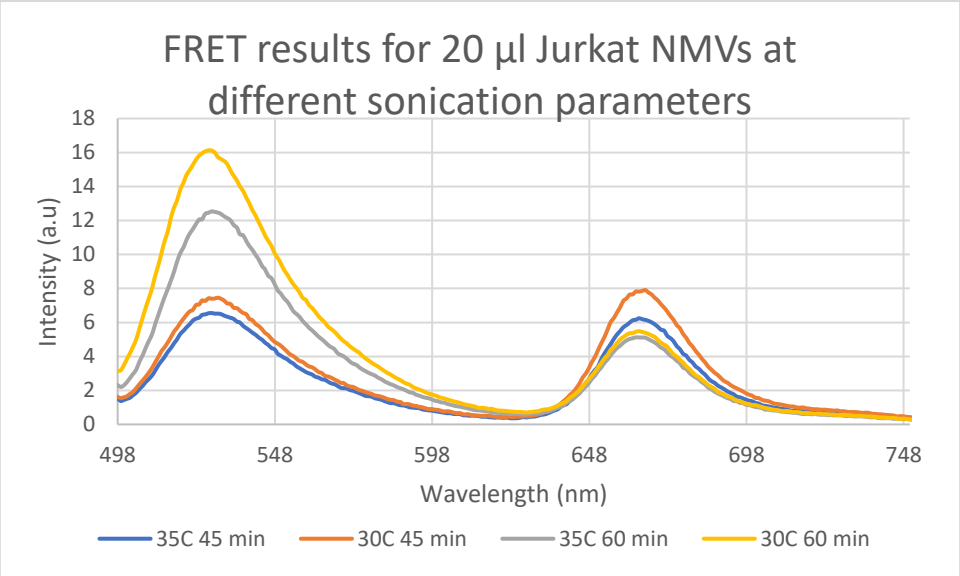

Figure 13: Intensity of the fluorescent emission, in arbitrary units, at different wavelengths in nm. Each curve represents the average of three FRET measurement from samples sonicated at a specific sonication parameter given below the graph. The first dominant peak is the emission peak of Oregon Green 488 (the donor fluorophore) at 526 nm, and the second dominant peak is the emission peak of Atto647 (the acceptor fluorophore) at 669 nm.

The peak values of the donor and acceptor peak for the sonicated samples are presented in table 4.

Table 3: A table summarizing the donor and acceptor peak values from the curves in figure 13, presented as mean value ± one standard deviation from three measurements.

Sonication parameter	**Donor peak value**	**Acceptor peak value**
35°C 45 min	6.51 ± 2.00	6.25 ± 2.05
30°C 45 min	7.41 ± 1.07	7.81 ± 0.95
35°C 60 min	12.50 ± 1.90	5.12 ± 1.76
30°C 60 min	14.95 ± 4.48	5.49 ± 1.39

From figure 13, the FRET ratio can be obtained by dividing the value at 669 nm from the donor peak, with the value at 526 nm from the acceptor peak. These values are presented in table 3 and 4. The FRET ratio is an indication of the amount of mixing that has occurred between the NMVs and the FRET vesicles. The FRET ratio for each set of sonication parameters are shown in figure 14.

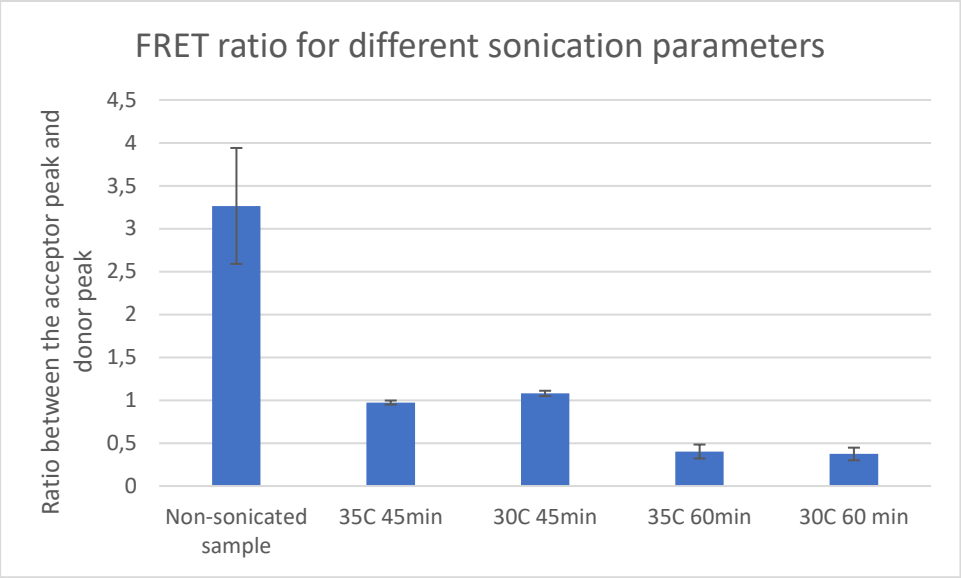

Figure 14: Graph showing the FRET ratio for each set of sonication parameters. From figures 12 and 13, the FRET ratio is obtained by dividing the maximum value of the donor peak, with the maximum value of the acceptor peak.

Changing the sonication time from 45 minutes to 60 minutes produces a larger change in FRET ratio compared to changing the temperature from 30˚C to 35˚C, suggesting sonication time affects the mixing process more than the temperature. One possibility is that the bath sonicator is more powerful than previously thought thus exerting a higher effect on the vesicles with longer sonication time.

The energy transfer between the two fluorophores is also depended on the functionality of the two molecules. To ensure that the FRET ratio in each case was not due to damaged acceptor fluorophores, the excitation wavelength was switched to 645 nm to solely excite the acceptor fluorophores. As in the case presented in figure 12, the measurement was performed on the samples *before* and *after* sonication and the results are presented in figure 15.

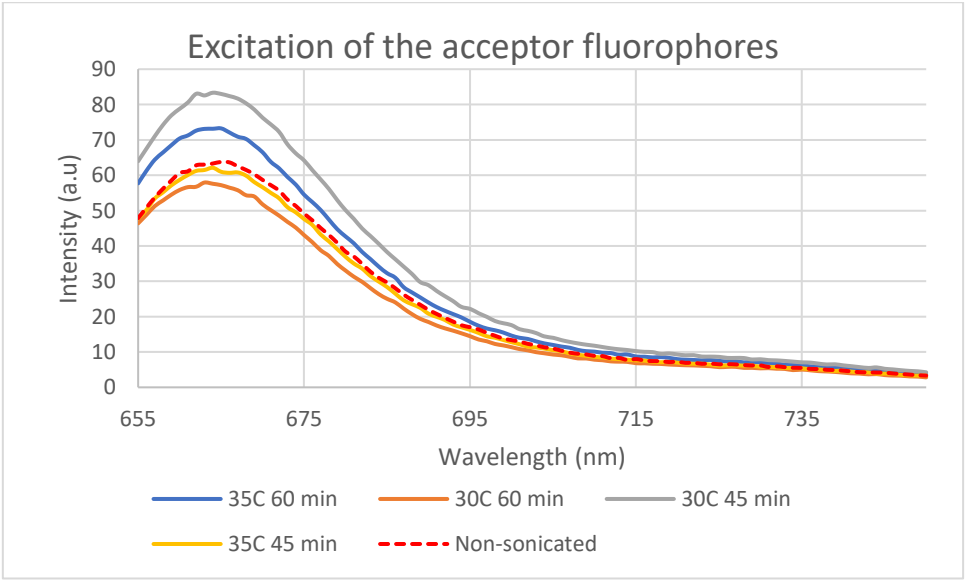

Figure 15: Excitation of only the acceptor fluorophores in a non-sonicated sample (left image), compared with sonicated samples at different conditions (right image). The excitation wavelength is 645 nm. The intensity is in arbitrary units, as a

function of wavelength in nm. The samples in both cases consisted of 20 µl NMVs, 1 µl FRET vesicles (1 mg/ml) and 279 µl HEPES buffer solution. The mean of the peak value is 67.29 ± 9.94.

The peak values of the acceptor peak for the sonicated samples, when just exciting the acceptor fluorophores, are presented in table 5.

The four curves in the right image of figure 15 have similar shape and values to the curve in the control sample, suggesting that sonicating with these four sets of parameters does not damage the fluorophores in a significant way. 35°C 45 min was therefore deemed to be the optimal sonication parameter since it was the middleground of the four sets of sonication parameters. The curves vary in their peak values which may be attributed to pipetting errors in the uptake of FRET vesicles used in each sonication experiment.

In the by Pace et al. the optimal sonication parameter was chosen to be 20°C 10 min (9). This difference shows the different effects sonication has on the vesicle depending on the equipment. Most likely the bath sonicator used in this work is weaker in terms of power compared to the bath sonicator used by Pace et al.

The results shown in figure 13 and 14 implies that it is possible to mix synthetic vesicles with NMVs.

6.2. FRAP and mobility measurements

Characterization of the nSLB was done by performing FRAP measurements on the bilayer. With the settings described in section 5.6. a region of the nSLB was bleached at $t = 14s$. As time progressed, the intensity of the bleached region slowly transitioned towards its initial intensity as shown in figure 16.

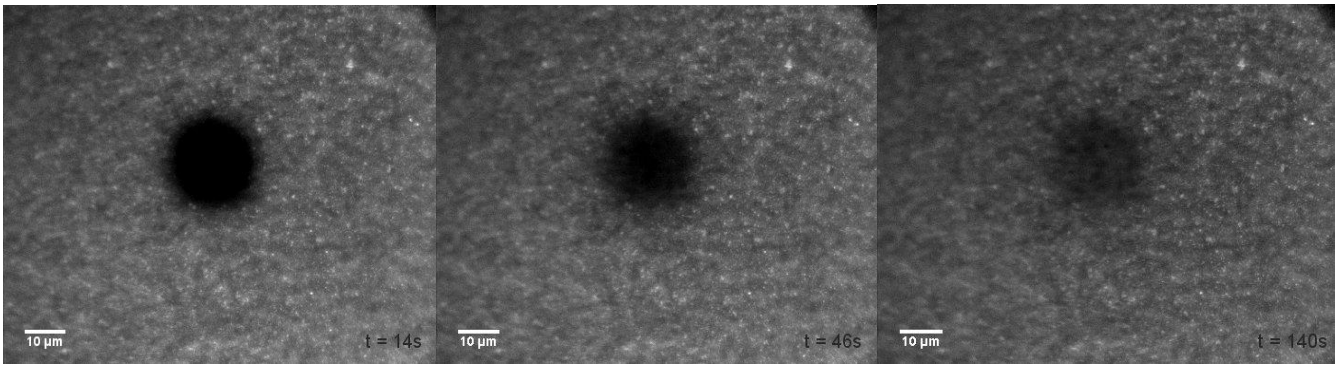

Figure 16: Three frames from a FRAP measurement performed on a nSLB labelled with Oregon Green 488. The frames are taken at different positions of time, showing the bleached spot undergoing recovery as one progresses from left to right. Each frame is marked with the corresponding time, t.

One additional way of visualizing the change in intensity in the bleached region is to plot the mean intensity of the bleached region as a function of time. The result is a *recovery curve* as shown in the right image of figure 17.

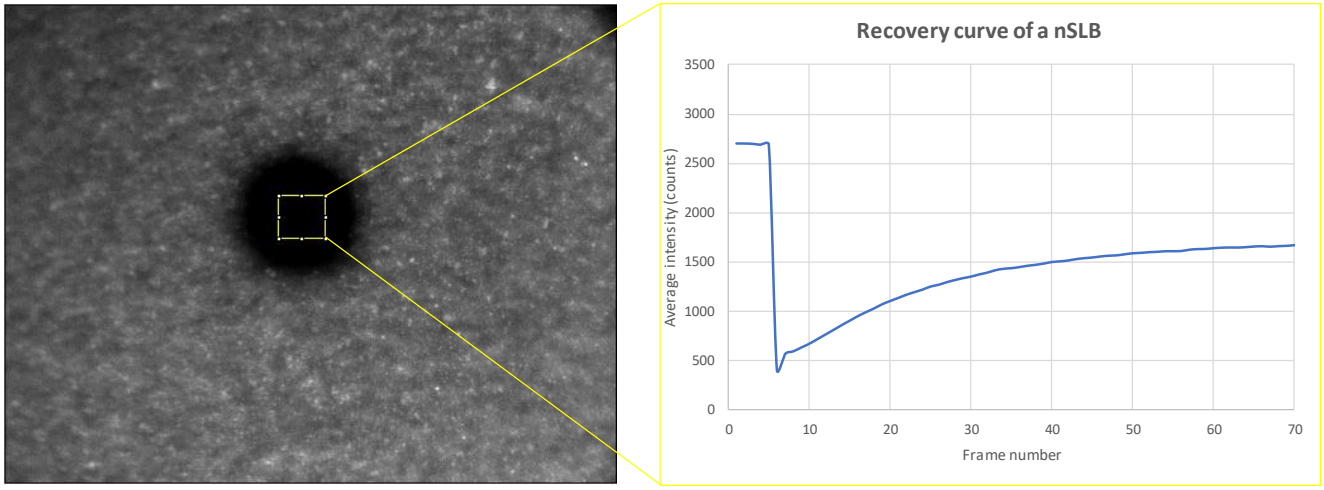

Figure 17: A recovery curve of the nSLB shown in figure 16. A region inside the bleached spot is marked, as shown in the left image, and the mean intensity (units in counts) of the region is shown in the right image as a function of the frame number.

Prior to the bleaching step, the marked region has a mean intensity of approximately *2600* counts. As the bleaching occurs the mean intensity drops to the background intensity value. After this point the mean intensity of the marked region starts to increase again with each frame. However, it is important to note that a full recovery of the intensity was never achieved which is related to an immobile fraction of lipids. Looking at figure 17 one can observe bright spots. Since the hybrid vesicles are labelled with OregonGreen488 these spots can be identified as *unruptured* vesicles. The failure to fully recover the initial intensity can partly be due to these vesicles since the bleaching step in FRAP does not distinguish between integrated lipids and lipids trapped in the bilayer of a vesicle. In addition, unruptured vesicles may act as obstacles for diffusing lipids in the nSLB.

The diffusion constant was calculated to *1.00 ± 0.07 μm²/s* as presented in table 3. This value was derived as an average of nine measurements obtained from three different nSLBs. Pace et al. reported a diffusion constant of 0.76 ± 0.11 $\mu m^2/s$ for the lipids. The difference could be attributed to a different sets of lipids and proteins being incorporated into the bilayer (9).

A PEG_POPC SLB (a SLB absent of NMV material) was made as a control sample. This SLB was also labelled with OregonGreen488 and by using FRAP the diffusion constant was found to be 1.20 ± 0.06 $\mu m^2/s$ (the value is an average of three measurements from one SLB). The diffusion constant of PEG_POPC bilayers have been reported to be 2.50 $\mu m^2/s$ by Reimhult et al. (35). Similar diffusion constants have also been encountered during this work, although multiple FRAP measurements were not taken for statistical reassurance in those bilayers. It is possible that this particular PEG_POPC SLB contains defects which leads to a lower diffusion constant.

Although, compared to the mobility in a nSLB, the coefficient is slightly lower. One explanation to this is that adding native cell membrane components increases the complexity of the bilayer. As discussed by Pace et al. the addition of NMV material includes the integration of large membrane proteins and sterol (such as cholesterol) which can lower the mobility for the fluorescent lipid-probe by acting as obstructions (9). Although the presence of PEG brushes elevates the nSLB above the glass substrate by 5-10 nm (35), some

membrane proteins may still have a large enough dimension where its interaction with the substrate is not eliminated by the PEG brushes. Any immobile lipids or proteins would act as stationary obstacles for the remaining components in the nSLB.

Table 4: A table presenting the calculated diffusion constants and the fraction of immobile lipids in the bilayer. The diffusion constant for the nSLB is presented as a mean ± one std from nine measurements, while the value for the PEG_POPC bilayer is the mean ± one std from three measurements.

Bilayer	**Diffusion constant (μm²/s)**	**Immobile Fraction**
nSLB	1.00 ± 0.07	0.21 ± 0.03
PEG_POPC	1.20 ± 0.06	0.05 ± 0.02

The immobile fraction for the nSLB was calculated to be 0.21 ± 0.03 as compared to the PEG_POPC SLB where the immobile fraction was equal to 0.05 ± 0.02. This could be an indication that there is a larger number of unruptured hybrid vesicles, compared to the number of unruptured synthetic vesicles which was reported by Pace et al. Protein-rich vesicles are less prone to fuse and rupture (9) and therefore a portion of the unruptured hybrid vesicles may be NMVs which did not undergo vesicle-vesicle fusion process during the sonication step.

Labelled lipids are not able to diffuse out of a bleached region if the lipids are still confined in the bilayer of an unruptured vesicle. To investigate this, the nSLB was labelled with the lipophilic tracer dye DiD. The result is shown in figure 18. Many bright spots are present in the bilayer which could correspond to unruptured vesicles due to a higher intensity from the DiD-labelled lipids not being able to diffuse in the bilayer. There is a noticeable number of unruptured vesicles which could explain the 21 % immobile fraction.

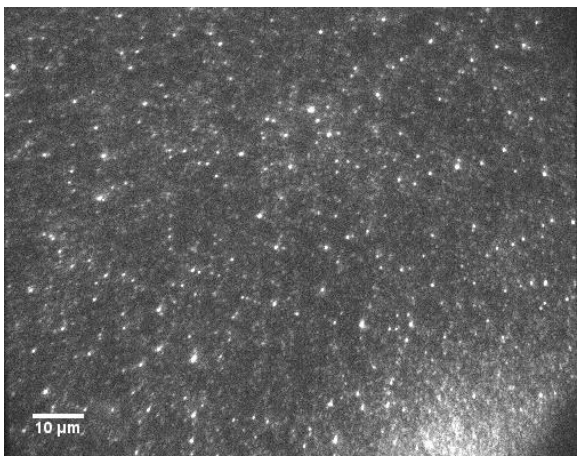

Figure 18: A nSLB has been labelled with DiD (diluted 100x) to highlight unruptured vesicles. The fluorescent dye labels all lipids.

6.3. Binding of antibodies

The results in section 6.2. suggest that a bilayer was formed from the vesicles in the sonicated samples. However, to investigate whether any native cell membrane components were actually integrated into the bilayer fluorescently-labelled antibodies specific for the T-cell proteins, presented in table 1, were used.

Figure 19 shows the result of the anti-TCR antibodies binding to the nSLB. There is clearly binding of the anti-TCR antibodies, however the question is whether they are also mobile. A FRAP measurement was performed to investigate this. The bleached spot in Figure 19 is recovering very slowly indicating that the TCR proteins seem to have a very low mobility. The diffusion constant was calculated to be 0.03 ± 0.01 $\mu m^2/s$ with immobile fraction of, 88 % ± 5 %. Thus, almost all of the antibodies, and thus TCR, seemed to be virtually immobile on the SLB. A possible explanation is that the TCR in the nSLB is interacting with the underlying substrate thus hindering its movement. Another possibility is that a majority of the TCR exists in unruptured vesicles and are not incorporated into the SLB.

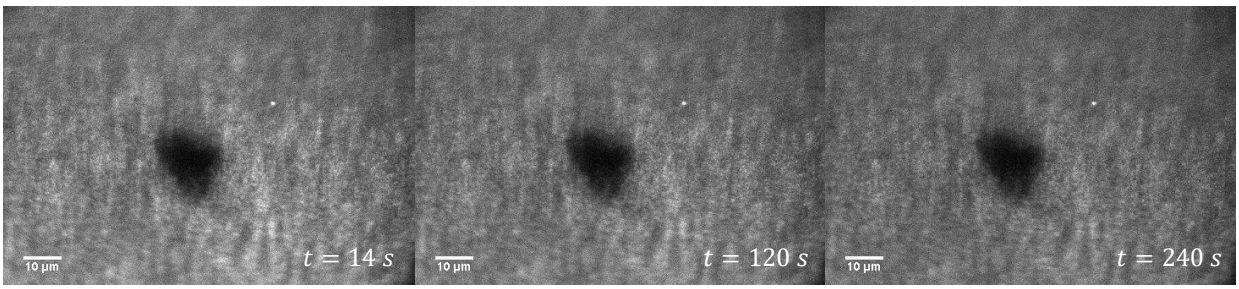

Figure 19: Three frames from a FRAP measurement on a nSLB labelled with the OKT3-antibody targeting TCR. A total of 120 frames were taken with two seconds apart.

An issue with the interpretability of this result also arises because of the possibility of unspecific binding. There could, be holes in the nSLB where the antibodies could adhere to the glass. A blocking agent, such as BSA, could be applied to prevent unspecific binding by the antibodies, before applying the antibodies of interest. However, other antibodies (as described below) did not show any noticeable binding to the nSLB at similar concentrations indicating that unspecific binding is small.

Anti-CD45 antibodies did also adhere to the nSLB as shown in Figure 20. As in the case of the anti-TCR antibodies the bleached spot does not recover much of its intensity (see also Figure 21). The immobile fraction was calculated to 97 ± 0.005 %, whereas the recovering fraction was too low to give a reliable diffusion constant.

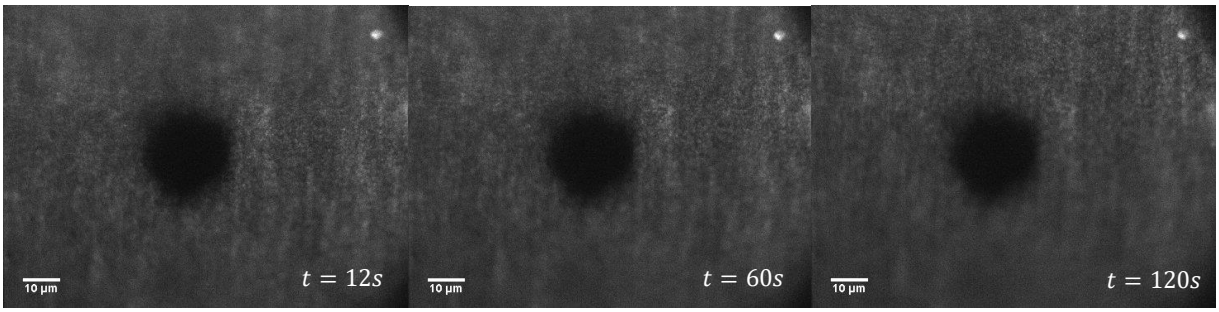

Figure 20: Three frames from a FRAP measurement on a nSLB labelled with anti-CD45 antibodies conjugated to Alexa Fluor 647. 60 frames were taken in total with two seconds apart. As time progresses, the bleached spot does not undergo a large recovery indicating that the proteins are largely immobile.

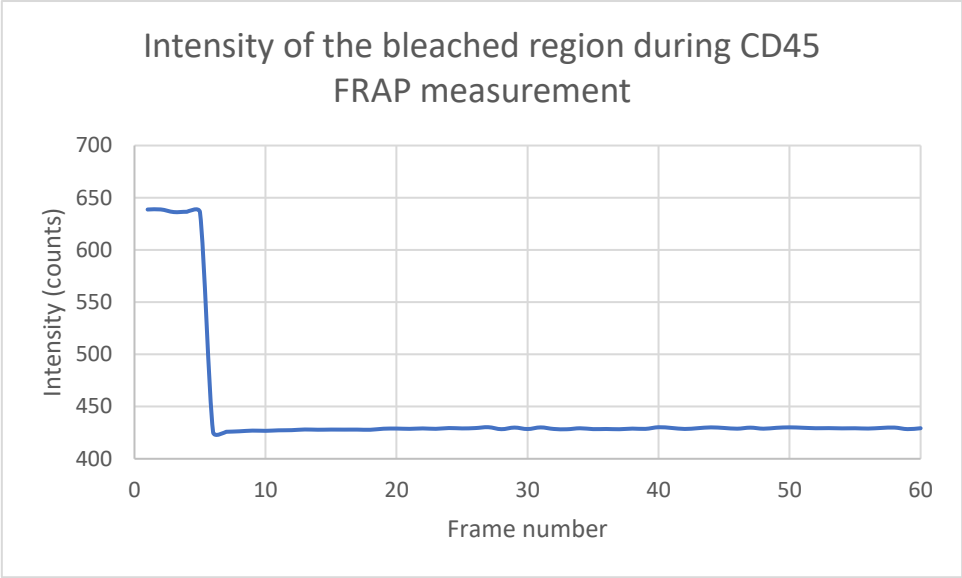

Figure 21: The recovery curve of the bleached region in figure 20. The mean intensity of that region is displayed for each frame. Upon bleaching of the antibodies specific for CD45 in a small region, the intensity in that region drops to a value similar to the background intensity. After this point, the region does not recover its initial intensity in a noticeable way.

A possible explanation for the immobility could be that the antibodies have bound to CD45 molecules still part of unruptured vesicles.

The low mobility could be attributed to the dimensions of CD45 which would result in the protein interacting too much with the glass substrate (these CD45 molecules are however, not detectable using antibodies due to binding site being in the ectoplasmic domain). A 3D-model of the cytoplasmic domains of CD45 was created and rendered using SwissProt (see, Figure 22):

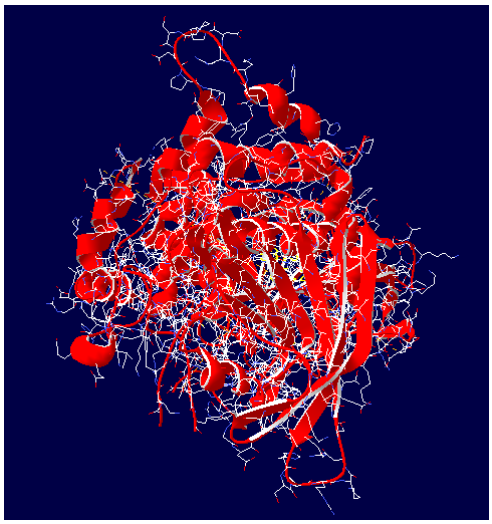

Figure 22: A 3D model of CD45's cytoplasmic domain, rendered using SwissProt (36).

Using the rendering programme, the height of the domain was found to be 6.4 nm and the width 5.3 nm. Considering that the PEG-brushes have a height between 5-10 nm (35) the cytoplasmic domain of CD45 is of similar dimensions as the PEG and could thus interact with

the glass substrate. Pace et al. did also see a significant drop in diffusivity of their studied transmembrane protein, *BACE1*, when having the ectoplasmic domain, of size 5 nm, facing the substrate (9). The diffusivity was reported to be 0.04 $\mu m^2/s$ with an immobile fraction of 30%. Thus, a larger fraction of the BACE1 proteins were able to recover, although slowly. Since both CD45 and TCR are larger molecules than BACE1 it is not unreasonable that they will experience a larger interaction with the substrate, thus slowing there mobility further.

Whether the immobility of the membrane proteins is due to confinement in unruptured hybrid vesicles/NMVs, or if the proteins are adsorbed to the substrate can not be extrapolated from the results. One possible experiment to conduct would be to use DiD-dye in combination with the antibodies. Overlapping of these two fluorescent signals in space would indicate the number of unruptured vesicles that contain membrane proteins. An immobile fraction of proteins is expected when studying the mobility of membrane proteins in a bilayer. As reported by Frick et al. an immobile fraction between 10 % and 20 % was found for all proteins in their study of protein mobility in membranes (37). Given therefore that the immobile fractions are so high for the membrane proteins in this work, it is more likely that the membrane proteins have not been integrated into the nSLB or that they are interacting with the substrate.

The other antibodies tested (anti-CD18, anti-CD2, anti-CD4, anti-MHC) showed almost no binding to the nSLB. An example is shown in Figure 23 using the anti-CD18 antibody. During the FRAP measurement, a very faint bleach spot was produced as shown in figure 23, which could just as well be from antibodies in solution that had not been rinsed away.

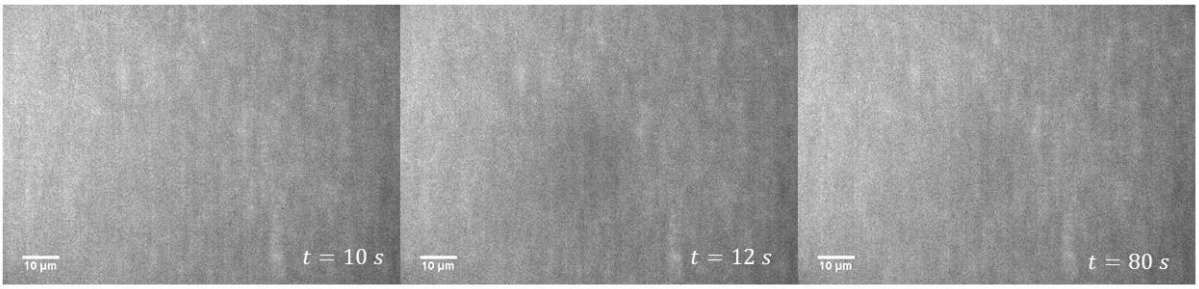

Figure 23: Three frames from a FRAP measurement on a nSLB labelled with anti-CD18 antibodies conjugated to FITC. The first image is taken after 10 s into the measurement and is the last frame before the bleaching of the antibodies. The second image is taken at 12 s, the first frame after the bleaching step, showing a faint black spot. The third image is taken at 80 s, showing an even fainter spot suggesting the region's intensity is recovering.

This indicates that either these proteins are not present in the bilayer, or that the proteins were damaged during sonication preventing them from binding to the antibodies. Alternatively, the PEG brushes might also act as steric hindrance for the antibodies to bind to their binding sites. Another possibility, which has been partly supported by separate experiments where these antibodies were bound to live T cell, is that these antibodies binds rather weakly, thus requiring a higher concentration to give a noticeable binding than was used in the experiments.

From the amount of anti-TCR and anti-CD45 bound to the nSLB it was also possible to estimate the molecular density of these proteins on the surface using equation [10]. The procedure is summarized in figure 24.

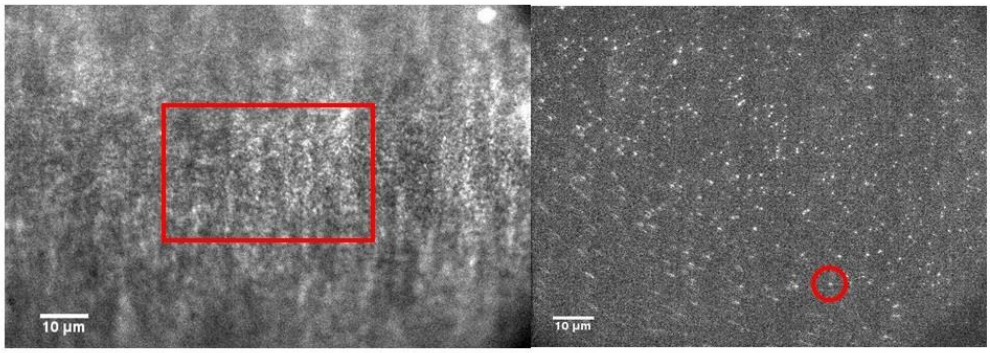

Figure 24: (Left image) A nSLB labelled with antibodies specific against CD45 with the center region marked with red. (Right image) A diluted sample of antibodies specific against CD45 with a single antibody marked by a red circle.

The right image of figure 24 was taken with a ND 1.3 filter and the 638-laser was operating at 100 mW. The left image of figure 24 was taken with a ND 2.0 filter and the laser was operating at 140 mW. The total intensity in the red square, was found to be $8.2 \cdot 10^5$ counts and is divided by the intensity from one single antibody, found to be 220 ± 20 counts, to obtain the concentration of antibodies, and therein the concentration of CD45, in the region. Given that each pixel is a square of length *0.22 µm*, the red square was found to have an area of 233 µm^2. The density of CD45 was then calculated to be *16 CD45 molecules/µm^2*. Previous studies report a molecular density of *2500 CD45 molecules/µm^2* in native T lymphocytes (38), making the density of CD45 on the nSLB approximately *0.6 %* of the molecular density in native cells. This value seems reasonable since approximately 10% of the vesicles used were native.

The same calculations could be done for TCR. However, the right dilution for the OKT3-antibodies could not be found to image single antibodies. In these calculations, it is assumed that the OKT3-antibodies have the same intensity as the anti-CD45 (220 ± 20 counts). Observation of the anti-TCR labelled bilayer was done so with a ND filter 1.3 and the 488-laser operating at 60 mW. A region of 165.38 µm^2 was found to have a total intensity of $3.5 \cdot 10^5$ counts. With the same pixel size and background intensity as for CD45, the concentration of TCR was calculated to be *9 TCR-molecules/µm^2*. The molecular density in native T lymphocytes has been reported as 150 TCR-molecules/µm^2 (38). This is equal to 6 % of the measured molecular density in native cells, which is reasonable considering that 10 % of the sonicated sample was comprised of NMVs.

7. Conclusion

To summarize the work, sonication parameters *35°C 45 min*, *30°C 45 min*, *35°C 60 min*, *30°C 60 min*, were evaluated to find the optimal one to ensure good formation of hybrid vesicles. The results suggest a bilayer was formed using the vesicles from the sonicated sample.

Characterization of the bilayer was then done to extrapolate the diffusion constant of the lipids in the bilayer as well as the investigating the presence of incorporated membrane proteins. Compared to SLBs devoid of any native material, the diffusion constant in a nSLB is slightly lower. This is likely attributed to the added complexity from the NMVs. A larger variety of lipids are present in the bilayer, as well as added membrane proteins each with a different diffusion constant which could act as a hindrance to the surrounding lipids.

Further characterization of the nSLB was done by using antibodies to characterize the membrane proteins in the nSLB. In total, six different antibodies were used. The FRAP measurements indicated the presence of *CD45* and *TCR* but not for *CD2*, *MHC*, *CD18* or *CD4*. It was found that the diffusion constant for the former proteins are low, and the immobile fraction is high. This could be explained by the proteins having very large cytoplasmic dimensions, causing them to interact and adhere to the glass substrate. In addition, many unruptured vesicles can be seen as bright spots on the images of the bilayer which could contribute to the high immobile fraction. A higher difficulty for vesicles with high protein content to rupture, compared to purely synthetic vesicles, was also reported by Pace et al. (9), in line with our results.

The failure of the antibodies to bind MHC, CD2, CD18 and CD4 could be an indication that either these proteins are damaged during sonication, or that the antibodies are not able to bind them. In the case of the proteins being damaged, a possible cause could be the preparation protocol of the NMVs being too aggressive. Alternatively, sonicating the vesicles samples at the newly-found optimal sonication parameters could in fact be too harsh on the proteins, in which case the test for membrane protein health (that is used in this work) needs to be re-evaluated. Antibodies not binding in to the intended target could be due to steric hindrance of the PEG brushes. The severity of this problem depends on whether the size of CD2, MHC and CD4 is comparable to the size of the PEG brushes, but also if the binding site for the antibodies are too close to the surface of the nSLB. Finally, if the concentration of the latter antibodies where increased significantly it might show more binding.

In summary, a protocol for nSLB formation from Jurkat T cells was developed and evaluated during this MSc project. Whereas the lipids in the nSLB are mobile it remains to be investigated how mobile, and well incorporated, different T-cell proteins are in the nSLB. The larger molecular complexes CD45 and TCR could be identified in the nSLB but with no significant mobility. This might not be a disadvantage for studies where only the interaction with the membrane protein is of interest and not its mobility, and could open up for new experiments where the large, and flat, contact area of the nSLB is utilized.

8. Future developments

Additional work can be done to alter the experimental protocol of forming the nSLBs to ensure a higher fraction of mobile proteins in the bilayer. PEG-brushes of higher molecular weight could be incorporated into the bilayer to increase the distance between the substrate and the bilayer. This could increase the mobility of the membrane proteins due to a decrease in the interaction between the proteins and the substrate. It would also be interest to form a nSLB absent of PEG-brushes to investigate whether they have any effect on the binding of antibodies. Ensuring as many of the membrane proteins, that are native to the T cell, are present in nSLB as well as having them being mobile increases the resemblance of this model membrane system to a native cell membrane. Once this is achieved, it would be of interest to investigate how well the nSLB mimics the cell membrane of a T cell. One way is to have the nSLB interact with other cells in the immune system to see whether the elicited response is similar to the response when the same experiment in conducted *in vivo*.

For example, as part of the development of the adaptive immune response, the B cell can present antigens to the T cell resulting in the B cell becoming triggered. Stimulation of the *B-cell antigen receptor* results in the production of IP_3. This molecule moves in the cytosol where it binds to IP_3 receptors in the endoplasmatic reticulum, which harbours internal pockets of Ca^{2+}-ions. Binding to the IP_3 receptors results in the release of Ca^{2+}-ions and the depletion of Ca^{2+}-ions activated calcium sensitive ion channels in the plasma membrane, causing an influx of Ca^{2+}-ions into the cytosol (39).

Since the nSLB in this work was made to mimic the cell membrane of T cells, it would be of interest to see whether B cells are triggered when deposited and bound to the surface of the nSLB. Activation of the B cells would then be characterized by an influx of Ca^{2+}-ions which would be observable through the use of a calcium-activated fluorescent dye. Similar work has been done to observe calcium release in Jurkat T cells when the cells are bound to CD2 molecules which have been attached to an artificial SLB (7).

References

1. Ashrafuzzaman, Mohammad, Jack A T. Membrane Biophysics. In: Membrane Biophysics. 2012. p. 151.

2. Overington JP, Al-Lazikani B, Hopkins AL. How many drug targets are there? Nat Rev Drug Discov. 2006;5(12):993–6.

3. Wurm C a, Neumann D, Schmidt R, Egner A, Jakobs S. Live Cell Imaging. Methods Mol Biol [Internet]. 2010;591(3):185–99. Available from: http://www.springerlink.com/index/10.1007/978-1-60761-404-3

4. Chan YHM, Boxer SG. Model membrane systems and their applications. Curr Opin Chem Biol. 2007;11(6):581–7.

5. Richter RP, Bérat R, Brisson AR. Formation of solid-supported lipid bilayers: An integrated view. Langmuir. 2006;22(8):3497–505.

6. Tamm LK, McConnell HM. Supported phospholipid bilayers. Biophys J. 1985;47(1):105–13.

7. Chang VT, Fernandes RA, Ganzinger KA, Lee SF, Siebold C, McColl J, et al. Initiation of T cell signaling by CD45 segregation at "close contacts." Nat Immunol. 2016;17(5):574–82.

8. Hardy GJ, Nayak R, Zauscher S. Model cell membranes: Techniques to form complex biomimetic supported lipid bilayers via vesicle fusion. Curr Opin Colloid Interface Sci [Internet]. 2013;18(5):448–58. Available from: http://dx.doi.org/10.1016/j.cocis.2013.06.004

9. Pace H, Simonsson Nyström L, Gunnarsson A, Eck E, Monson C, Geschwindner S, et al. Preserved Transmembrane Protein Mobility in Polymer-Supported Lipid Bilayers Derived from Cell Membranes. Anal Chem. 2015;87(18):9194–203.

10. Edidin M. Lipids on the frontier: A century of cell-membrane bilayers. Nat Rev Mol Cell Biol. 2003;4(5):414–8.

11. Singer SJJ, Nicolson GLL. The fluid mosaic model of the structure of cell membranes. Science (80-). 1972;175(4023):720–31.

12. Parkin J, Cohen B. Overview of the Immune System. Lancet [Internet]. 2001;357:1777–89. Available from: http://www.msdmanuals.com/en-gb/professional/immunology-allergic-disorders/biology-of-the-immune-system/overview-of-the-immune-system

13. Bromley SK, Burack WR, Kenneth G, Somersalo K, Sims TN, Sumen C, et al. The Immunological Synapse. 2001;

14. Huppa JB, Davis MM. T-cell-antigen recognition and the immunological synapse. Nat Rev Immunol [Internet]. 2003;3(12):973–83. Available from: http://www.nature.com/doifinder/10.1038/nri1245

15. Abraham RT, Weiss A. Jurkat T cells and development of the T-cell receptor signalling paradigm. Nat Rev Immunol [Internet]. 2004;4(4):301–8. Available from: http://www.nature.com/doifinder/10.1038/nri1330

16. Seu KJ, Pandey AP, Haque F, Proctor EA, Ribbe AE, Hovis JS. Effect of surface treatment on diffusion and domain formation in supported lipid bilayers. Biophys J. 2007;92(7):2445–50.

17. Reimhult E, Kasemo B, Höök F. Rupture pathway of phosphatidylcholine liposomes on silicon dioxide. Int J Mol Sci. 2009;10(4):1683–96.

18. Jackman JA, Kim MC, Zhdanov VP, Cho N-J. Relationship between vesicle size and steric

hindrance influences vesicle rupture on solid supports. Phys Chem Chem Phys [Internet]. 2016;18(4):3065–72. Available from: http://xlink.rsc.org/?DOI=C5CP06786C

19. Weirich KL, Israelachvili JN, Fygenson DK. Bilayer edges catalyze supported lipid bilayer formation. Biophys J [Internet]. 2010;98(1):85–92. Available from: http://dx.doi.org/10.1016/j.bpj.2009.09.050

20. Andersson J, Köper I. Tethered and polymer supported bilayer lipid membranes: Structure and function. Membranes (Basel). 2016;6(2).

21. Ye Q, Konradi R, Textor M, Reimhult E. Liposomes tethered to omega-functional PEG brushes and induced formation of PEG brush supported planar lipid bilayers. Langmuir. 2009;25(23):13534–9.

22. Willem M, Garratt AN, Novak B, Citron M, Kaufmann S, Rittger A, et al. Control of peripheral nerve myelination by the beta-secretase BACE1. Science. 2006;314(5799):664–6.

23. W.Davidson M. Resolution | MicroscopyU [Internet]. [cited 2018 Apr 20]. Available from: https://www.microscopyu.com/microscopy-basics/resolution

24. Kremers G-J, Piston D., Davidson M. Basics of FRET Microscopy | MicroscopyU [Internet]. [cited 2018 Apr 13]. Available from: https://www.microscopyu.com/applications/fret/basics-of-fret-microscopy

25. Seifert U, Lepowsky R. Chapter 8 Morphology of vesicles. Handb Biol Phys. 1995;1(C):403–63.

26. Stillwell W. An Introduction to Biological Membranes: From bilayers to rafts. 2013. 288 p.

27. Herman B. Fluorescence Microscopy. Curr Protoc Cell Biol. 1998;1–10.

28. Spring KR, Davidson MW. Introduction to Fluorescence Microscopy | MicroscopyU [Internet]. [cited 2018 Apr 26]. Available from: https://www.microscopyu.com/techniques/fluorescence/introduction-to-fluorescence-microscopy

29. Fish KN. (TIRF) Microscopy. Curr Protoc Cytom. 2009;(October):1–13.

30. Lopez A, Dupou L, Altibelli A, Trotard J, Tocanne JF. Fluorescence recovery after photobleaching (FRAP) experiments under conditions of uniform disk illumination. Critical comparison of analytical solutions, and a new mathematical method for calculation of diffusion coefficient D. Biophys J. 1988;53(6):963–70.

31. Anderson ME, Siahaan TJ. Targeting ICAM-1 LFA-1 interaction for controlling autoimmune diseases: designing peptide and small molecule inhibitors. Elsevier. 2003;(Peptides 24):487–501.

32. Swanberg E. Supported Lipid Bilayers Derived From Antigen Presenting Cells. Chalmers, Univ Technol. 2016;

33. Edelstein AD, Tsuchida MA, Amodaj N, Pinkard H, Vale RD, Stuurman N. Advanced methods of microscope control using μManager software. J Biol Methods [Internet]. 2014;1(2):10. Available from: http://www.jbmethods.org/jbm/article/view/36

34. Jönsson P, Jonsson MP, Tegenfeldt JO, Höök F. A method improving the accuracy of fluorescence recovery after photobleaching analysis. Biophys J. 2008;95(11):5334–48.

35. Kaufmann S, Papastavrou G, Kumar K, Textor M, Reimhult E. A detailed investigation of the formation kinetics and layer structure of poly(ethylene glycol) tether supported lipid bilayers. Soft Matter [Internet]. 2009;5(14):2804. Available from: http://xlink.rsc.org/?DOI=b901874c

36. UniProt. UniProtKB - P08575 (PTPRC_HUMAN) [Internet]. Available from: http://www.uniprot.org/uniprot/P08575

37. Frick M, Schmidt K, Nichols BJ. Modulation of Lateral Diffusion in the Plasma Membrane by Protein Density. Curr Biol. 2007;17(5):462–7.

38. Johnson KG, Bromley SK, Dustin ML, Thomas ML. A supramolecular basis for CD45 tyrosine phosphatase regulation in sustained T cell activation. Proc Natl Acad Sci U S A [Internet]. 2000;97(18):10138–43. Available from: http://www.pubmedcentral.nih.gov/articlerender.fcgi?artid=27752&tool=pmcentrez&rendertype=abstract

39. Baba Y, Kurosaki T. Role of Calcium Signaling in B Cell Activation and Biology. In: Kurosaki T, Wienands J, editors. B Cell Receptor Signaling [Internet]. Cham: Springer International Publishing; 2016. p. 143–74. Available from: https://doi.org/10.1007/82_2015_477